Published in final edited form as:

Dev Cell. 2023 May 08; 58(9): 791–805.e4. doi:10.1016/j.devcel.2023.03.009.

Prerequisite endocardial-mesenchymal transition for murine cardiac trabecular angiogenesis

Pengfei Lu[1,2,*], **Bingruo Wu**[1], **Yidong Wang**[1,3], **Megan Russell**[1], **Yang Liu**[1], **Daniel J. Bernard**[4], **Deyou Zheng**[1,5], **Bin Zhou**[1,6,7,*]

[1]Department of Genetics, Albert Einstein College of Medicine, Bronx, New York, NY 10461, USA

[2]Precision Research Center for Refractory Diseases, Institute for Clinical Research, Shanghai General Hospital, Shanghai Jiao Tong University School of Medicine, Shanghai 201620, China

[3]Cardiovascular Research Center, School of Basic Medical Sciences, Jiaotong University, Xi'an 710061, China

[4]Department of Pharmacology and Therapeutics, McGill University, Montreal, QC H3G 1Y6, Canada

[5]Departments of Neurology and Neuroscience, Albert Einstein College of Medicine, Bronx, New York, NY 10461, USA

[6]Departments of Pediatrics and Medicine, Albert Einstein College of Medicine, Bronx, New York, NY 10461, USA

[7]Lead contact

SUMMARY

Coronary heart disease damages the trabecular myocardium, and the regeneration of trabecular vessels may alleviate ischemic injury. However, the origins and developmental mechanisms of trabecular vessels remain unknown. Here, we show that murine ventricular endocardial cells generate trabecular vessels through an "angioEMT" mechanism. Time course fate mapping defined a specific wave of trabecular vascularization by ventricular endocardial cells. Single-cell transcriptomics and immunofluorescence identified a subpopulation of ventricular endocardial cells that underwent endocardial-mesenchymal transition (EMT) before these cells generated trabecular vessels. *Ex vivo* pharmacological activation and *in vivo* genetic inactivation experiments identified an EMT signal in ventricular endocardial cells involving SNAI2-TGFB2/TGFBR3, which was a prerequisite for later trabecular-vessel formation. Additional loss- and gain-of-function genetic studies showed that VEGFA-NOTCH1 signaling regulated post-EMT

[*]Correspondence: pfluxury@gmail.com (P.L.), bin.zhou@einsteinmed.edu (B.Z.).

AUTHOR CONTRIBUTIONS

P.L. and B.Z. conceived the study. P.L. and B.Z. designed the experiments. P.L., B.W., and Y.W. conducted experiments. D.J.B. provided the floxed *Tgfbr3* mouse line. P.L., B.W., Y.W., M.R., Y.L., D.Z., and B.Z. analyzed the data. P.L. and B.Z. wrote the manuscript. B.Z. supervised experiments and provided grant support.

DECLARATION OF INTERESTS

The authors declare no competing interests.

SUPPLEMENTAL INFORMATION

Supplemental information can be found online at https://doi.org/10.1016/j.devcel.2023.03.009.

trabecular angiogenesis by ventricular endocardial cells. Our finding that trabecular vessels originate from ventricular endocardial cells through a two-step angioEMT mechanism could inform better regeneration medicine for coronary heart disease.

In brief

Lu et al. identify two waves of coronary-vessel formation at trabecular and compact myocardium of the murine heart. Their work finds that trabecular vessels arise from ventricular endocardial cells and characterizes a two-step angioEMT mechanism underlying the process that may inform better regeneration medicine for coronary heart disease.

Graphical Abstract

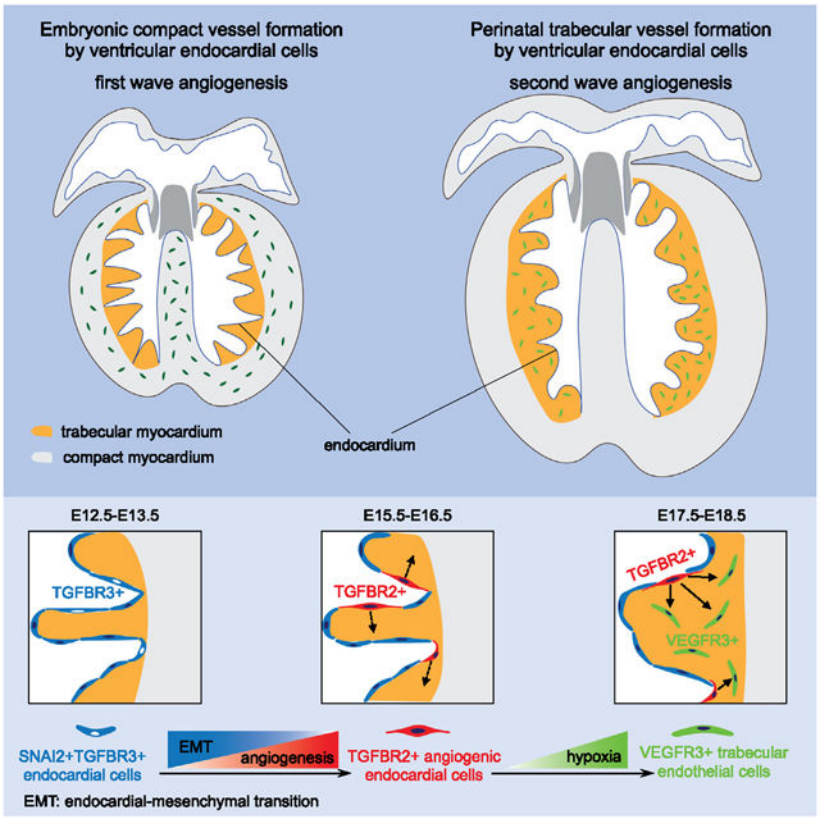

INTRODUCTION

The coronary circulation supplies blood to the heart muscle. Disrupted coronary circulation leads to ischemic heart disease that is often confined to the subendocardial layer of the left ventricular wall.[1] This layer consists of trabecular myocardium.[2,3] Hence, the targeted rebuilding of coronary circulation at the trabecular myocardium, i.e., regeneration of trabecular vessels, may represent a promising cell therapy for coronary heart disease, which remains as the leading cause of death worldwide.[4,5] However, little is known on how trabecular vessels are formed during development. This lack of knowledge has limited

our ability to design an effective and cell-type-specific therapy for coronary heart disease through regenerating trabecular vessels following the developmental paradigm.[6,7]

Coronary vessels at compact myocardium are derived from ventricular endocardial cells,[8–12] sinus venous endothelial cells (ECs),[13] and proepicardial cells.[14,15] These progenitor cell populations give rise to compact coronary vessels in a spatially complementary manner through distinct mechanisms.[8,9,11,16–18] In contrast, the developmental origins and mechanisms of trabecular vessels remain unknown. In this study we addressed this knowledge gap using an integrated approach of cell lineage tracing, single-cell RNA sequencing (scRNA-seq) analysis, *ex vivo* coronary angiogenesis assays, and *in vivo* gain- and loss-of-function validations.

We found two (i.e., first and second) waves of coronary vascularization at compact and trabecular myocardium, respectively, by ventricular endocardial cells. We identified a previously unknown endocardial-mesenchymal transition (EMT) mechanism through which a subset of ventricular endocardial cells is primed before they generate trabecular vessels by angiogenesis. We further characterized a sequential signaling event involved in snai family zinc finger 2 (SNAI2)-transforming growth factor beta receptor 2 (TGFB2)/transforming growth factor beta receptor 3 (TGFBR3) during EMT and vascular endothelial growth factor-A (VEGFA)-notch receptor 1 (NOTCH1) during subsequent angiogenesis, which is required for the second wave of coronary-vessel formation at trabecular myocardium. Our finding that trabecular vessels originate from ventricular endocardial cells through a two-step angioEMT (angiogenesis following EMT) mechanism could inform better regeneration medicine for coronary heart disease.

RESULTS

Formation of trabecular vessels requires myocardial VEGFA

To characterize coronary-vessel formation at trabecular myocardium, we performed double immunostaining on serial sections of mouse embryonic heart from embryonic day (E) 14.5 to E18.5 using antibodies against a panendothelial marker expressed by the coronary endothelium and ventricular endocardium (PECAM1) and an endothelial protein expressed by angiogenic cells (VEGFR3).[9,10] We found that few if any coronary plexuses were present at trabecular myocardium before E16.5 (Figure 1A). In contrast, coronary plexuses began to emerge at trabecular myocardium around E16.5–17.5; these newly formed trabecular vessels expressed VEGFR3 and expanded quickly, leading to significantly increased vascular density at trabecular myocardium around birth (Figures 1A and 1B). The vascular expansion was accompanied by thickening of the trabecular myocardium. The high level of VEGFR3 expression in these forming trabecular vessels suggests that angiogenic proliferation drives trabecular-vessel formation in the perinatal heart.

As hypoxia induces angiogenesis during vascular development[19–21] and myocardial hypoxia is intimately associated with developmental coronary angiogenesis at compact myocardium,[8,9] we investigated hypoxia at trabecular myocardium of the developing heart using hypoxia-probe staining.[22] endomucin (EMCN) was co-stained to mark the ventricular endocardium to visualize trabecular and compact myocardium. No hypoxic signaling was

detected at trabecular myocardium before E16.5 (Figures 1C and 1D). In contrast, we detected hypoxic signaling at trabecular myocardium from E17.5 to 2 days post-natal (P2), which increased over time (Figures 1C and 1D). The coordinated myocardial hypoxia and coronary plexus formation at trabecular myocardium suggest that trabecular-vessel development is dependent on the hypoxia-regulated VEGFA signaling.[8,9,11]

We tested this hypothesis by timed deletion of *Vegfa* in the myocardium through crossing the *Tnnt2*^{MerCreMer} deleter[23] with the floxed *Vegfa* mouse.[24] We inactivated *Vegfa* expression by administrating tamoxifen at E17.5 when trabecular myocardium became hypoxic. We examined the myocardial *Vegfa* null heart (*Vegfa*^{cKO} hereafter) at P7 and found that the *Vegfa*^{cKO} heart became severely hypoxic, especially at trabecular myocardium, compared with the littermate control heart (*Vegfa*$^{f/f}$) (Figures 1E–1H and S1A). Further PECAM1 immunostaining identified significantly reduced density of coronary vessels at both trabecular and compact myocardium of the *Vegfa*^{cKO} heart compared with the control *Vegfa*$^{f/f}$ heart (Figures 1I–1L and S1B). The decrease was more pronounced at trabecular myocardium. This demonstrates that trabecular-vessel formation requires myocardial VEGFA signaling and suggests that reduced trabecular vascularization escalates hypoxia at trabecular myocardium.

Ventricular endocardial cells give rise to trabecular vessels

Previous studies have shown that coronary vessels at compact myocardium have developed before coronary circulation begins at E14.5 and they arise from the progenitor cells at the sinus venous endothelium[13] around E9.5 and the ventricular endocardium[8] around E11.5. However, the developmental origins of trabecular vessels were not specifically examined in these studies. Therefore, we performed a lineage tracing analysis of ventricular endocardial cells using the inducible endocardial Cre line *Npr3*^{CreERT2}.[10] *Npr3* is predominantly expressed in the entire ventricular endocardium from E10.5 to E16.5, as shown by immunostaining using antibodies against natriuretic peptide receptor 3 (NPR3) (Figure S2).

We labeled ventricular endocardial cells by the administration of tamoxifen to dams at E10.5, when sinus-venosus-derived coronary progenitors had already migrated onto the surface of the ventricle[13] but ventricular endocardial cells had yet to undergo coronary angiogenesis.[8] We then examined E16.5 heart by costaining for the lineage marker GFP and the endothelial marker platelet/endothelial cell adhesion molecule 1(PECAM1). The result showed that GFP-labeled progenies of E10.5 ventricular endocardial cells contributed to entire coronary vessels at the interventricular septum and part of coronary vessels at compact myocardium of the ventricles (Figures 2A and 2B).

In contrast, when we induced the labeling at E12.5, GFP-expressing progenies of E12.5 ventricular endocardial cells were found in coronary vessels at the interventricular septum of E16.5 heart, but not in coronary vessels at compact myocardium of the ventricles (Figures 2C and 2D). This is consistent with our immunostaining observations (Figures 1A and 1B), showing no sign of coronary-vessel formation at trabecular myocardium by E16.5. These results support that a subset of ventricular endocardial cells is committed to the coronary endothelial fate before E12.5.[8] *Npr3*^{CreERT2} induced at E10.5 may label some epicardial

cells; however, this does not interfere with lineage tracing analysis of ventricular endocardial cells, as epicardial cells labeled by *Npr3*^{CreERT2} do not become coronary ECs.[10,15,25]

Because trabecular vessels emerged after E16.5 (Figures 1A and 1B), we next examined P7 hearts following the labeling of ventricular endocardial cells at E10.5, and we found that progenies of E10.5 ventricular endocardial cells contributed to entire coronary vessels at trabecular myocardium (Figures 2E and 2F). Trabecular vessels completely labeled by GFP were clearly separated from the coronary vessels at compact myocardium, which were partially labeled by GFP. This labeling pattern suggests that after E16.5, trabecular vessels likely arise directly from ventricular endocardial cells. This is supported by the observation that ventricular endocardial cells labeled at E12.5 give rise to entire trabecular vessels but have no contribution to vessels developed at compact myocardium (Figures 2G and 2H). Lineage tracing results from E16.5 and P7 hearts labeled at E10.5 and E12.5, respectively, demonstrate two waves of coronary-vessel formation by ventricular endocardial cells (Figure 2I). The first wave of coronary plexuses occurs at compact myocardium around E10.5, performed by earlier ventricular endocardial cells that give rise to part of compact myocardium vessels. The second wave of coronary plexuses occurs after E16.5 at trabecular myocardium by later ventricular endocardial cells that generate entire trabecular vessels.

Characterization of the second-wave progenitor cells in ventricular endocardium

To determine when second-wave progenitor cells in ventricular endocardium are committed to trabecular vessels, we labeled ventricular endocardial cells with GFP in the *Npr3*^{CreERT2};*R26*^{fsGFP} embryos at different stages from E10.5 to E16.5. When inducing GFP labeling with tamoxifen at E10.5 or E11.5, GFP-labeled progenies of ventricular endocardial cells were found in all trabecular vessels expressing PECAM1 and some coronary vessels at compact myocardium of P7 hearts (Figures 3A, 3B, S3A, and S3B). In contrast, when inducing GFP labeling at E12.5, GFP-labeled progenies of ventricular endocardial cells were found in all trabecular vessels of P7 hearts, but few if any coronary vessels in compact myocardium (Figures 3C and S3C). The contribution of GFP-labeled progenies of E13.5–E14.5 ventricular endocardial cells to trabecular vessels of P7 hearts was gradually decreased (Figures 3D, 3E, S3D, and S3E), suggesting reduced potential for the endocardial-to-endothelial fate change. By E16.5, ventricular endocardial cells largely lost this potential as few GPF-labeled progenies derived from ventricular endocardial cells were present in trabecular vessels (Figures 3F and S3F).

Quantitative analysis of the lineage data confirmed that the potential for commitment to the trabecular-vessel fate by ventricular endocardial cells was downregulated from E12.5 to E16.5 and limited to this window (Figure 3G). This is consistent with our previous observations that ventricular endocardial cells of E17.5 hearts have completely lost their angiogenic potential to form coronary vessels.[10] In contrast, the commitment of ventricular endocardial cells to coronary vessels at compact myocardium was restricted to the earlier developmental stage, E10.5–E12.5 (Figure 3H). The overall commitment of ventricular endocardial cells to coronary vessels at the entire left ventricle was reduced from E10.5 to E16.5 (Figure 3I).

To visualize the second wave of coronary-vessel formation by ventricular endocardial cells, we chose to label ventricular endocardial cells at E12.5 by *Npr3*^{CreERT2}. These cells exclusively contributed to trabecular vessels from the second wave but did not participate in the first wave that gave rise to coronary vessels at compact myocardium. We examined the forming trabecular vessels of the perinatal heart by GFP-labeled progenies derived from E12.5 ventricular endocardial cells. In E16.5 heart, all GFP-labeled cells were located within ventricular endocardium, and few if any GFP-labeled cells were present in coronary vessels at compact or trabecular myocardium expressing PECAM1 (Figure 3J). In the E17.5 heart, some GFP-labeled trabecular vessels began to emerge at the base of trabecular crypts (Figure 3K, arrowheads). The number of GFP-labeled vessels increased and expanded toward the center of trabecular crypts by E18.5 (Figure 3L, arrowheads). From P0 to P7, the number of GFP-labeled trabecular vessels increased continuously and some extended into the newly compacted myocardium from the trabeculae (Figures 3M, 3N, S3G, and S3H).

Quantitative analysis of the developmental lineage data showed increased density of GFP-labeled trabecular vessels over time from E16.5 to P7 (Figure 3O) and increased proportion of second-wave-generated vessels in entire coronary vessels of the left ventricle (Figure 3P). The lineage tracing results demonstrate that a subset of ventricular endocardial cells is committed to the trabecular-vessel fate between E12.5 and E16.5, and these progenitor cells vascularize trabecular myocardium only after E16.5, likely in response to the hypoxic myocardium occurring at birth.

Sequential EMT and angiogenesis actions by ventricular endocardial cells

Because the potential of ventricular endocardial commitment to the trabecular-vessel fate is developmentally reduced from E12.5 to E16.5, we performed scRNA-seq analysis on E12.5, E13.5, E14.5, and E15.5 hearts. For each stage, we obtained 4,073–9,092 cells of high quality after strict quality control and filtering (Figures S4A and S4B). We integrated the cells from all four stages, including duplications for E13.5, E14.5, and E15.5 and clustered them based on their similar gene expression profiles (Figure 4A). The analysis identified an EC cluster based on the high expression of endothelial markers *Cdh5* and *Pecam1* (Figures 4B and S4C). We also identified cell clusters for cardiomyocytes (CMs) (Figure S4D), cardiac fibroblast and mesenchyme (Figure S4E), and macrophages (Figure S4F).

To focus on ECs, we further clustered the EC cluster into six subclusters and determined the marker genes for each subcluster. This allowed us to identify cluster 1 as valve ECs (*Cldn11*$^{+}$; *Wnt4*$^{+}$), cluster 2 as coronary ECs (*Fabp4*$^{+}$; *Dll4*$^{+}$), and cluster 5 as lymphatic ECs (*Lyve1*$^{+}$; Prox1^{+}), whereas clusters 0, 3, and 4 were identified as endocardial cells expressing endocardial genes *Npr3* and *Adgrg6*. Cluster 0 is the main endocardial cell cluster, whereas cluster 3 is a proliferating endocardial cell cluster (Figures 4D, S4G, and S4H), and cluster 4 has a small number of cells (<3% of the total endocardial cells (Figure S4I). However, these cells formed a distinct cluster by unbiased clustering analysis, suggesting unique functions.

Because we found that ventricular endocardial cells were the progenitor source of trabecular vessels, we next compared cluster 0 and 4 endocardial cells along with cluster 2 coronary ECs. We found that cluster 4 cells showed lower expression of endocardial markers *Npr3*

and *Adgrg6* when compared with cluster 0 (Figure 4D). We further noticed that cluster 4 expressed a group of key EMT regulatory genes such as *Snai2*, *Sox9*, and *Tbx20*, which were not expressed by most of endocardial cells, i.e., cluster 0, or coronary ECs, i.e., cluster 2 (Figure 4D). Comparing expression profiles of endocardial and coronary endothelial marker genes and essential EMT regulatory genes in cluster 0 and 4 endocardial cells and cluster 2 coronary ECs indicated that EMT was a unique function of cluster 4 (Figure 4E).

As the transforming growth factor beta (TGF-β) pathway plays a key role in EMT, we examined the expression of ligands and receptors of TGF-β signaling and found that *Tgfb1* was expressed in coronary endothelium (cluster 2) and endocardium (clusters 0 and 4); *Tgfb2* was expressed in CMs and endocardial cell clusters (clusters 0 and 4); and *Tgfb3* was specifically expressed in cluster 4 endocardial cells (Figure 4F). Among the TGF-β receptors, *Tgfbr1* was expressed in cardiomyocytes and cluster 4 endocardial cells, *Tgfbr2* was expressed in both endocardial and coronary ECs, and *Tgfbr3* was specifically expressed in endocardial cells (clusters 0 and 4) (Figure 4F). Further ligand-receptor interaction analysis using CellChat[26] supported strong *Tgfb2-Tgfbr2/3* interactions between cardiomyocytes (CMs) and endocardial cells (clusters 0 and 4), and *Tgfb1-Tgfbr1/2* interactions between coronary ECs (cluster 2) and endocardial cells (cluster 4) (Figure 4G). These findings suggest that TGF-β-dependent EMT via myocardial TGF-β2-endocardial TGF-βR2/3 occurs in a subset of chamber endocardial cells.

We next performed the pseudotime trajectory analysis among endocardial clusters 0 and 4 and coronary endothelial cluster 2. We found that endocardial cluster 4 was an intermediated state between endocardial cells (cluster 0) and coronary ECs (cluster 2) (Figure 5A). Further differential expression analysis of endocardial cells (between clusters 0 and cluster 4) identified the regulatory EMT genes (*Tbx20*,[27] *Gsn*,[28] *Sox9*,[29] and *Twist1*[30]) were upregulated in cluster 4 endocardial cells when compared with cluster 0 (Figure S4J). On the other hand, endocardial genes (*Npr3*, *Plvap*, and *Emcn*) were downregulated in cluster 4 when compared with cluster 0 endocardial cells (Figure S4J).

Because of the small cell numbers in cluster 4 that prevented us from more comprehensive analysis, we overcame this limitation by comparing the main endocardial cells (cluster 0) among the four stages from E12.5 to E15.5 to further identify the developmental potential of endocardial commitment to the trabecular-vessel fate. Differential gene expression analysis over these time points showed that genes involved in EMT were downregulated, whereas genes involved in angiogenesis were upregulated from E12.5 to E15.5 (Figures 5B and 5C). Gene ontology (GO) and Kyoto Encyclopedia of Genes and Genomes (KEGG) pathway analyses for the genes significantly downregulated from E12.5 to E15.5 showed that RNA splicing and cell cycle were among the most highly enriched functions, reflecting the maturation of ventricular endocardial cells (Figure 5D). Notably, EMT was also among the enriched functions, including known the EMT genes *Tgfbr3* and *Tbx20* (Figures 5D and 5E).

We therefore sought to validate the potential role of EMT in the formation of trabecular vessels. We first examined the expression of *Tgfbr3* in E12.5, E14.5, and E16.5 hearts by immunostaining, as it is required for coronary-artery formation.[31] Our results confirmed

that *Tgfbr3* was specifically expressed in ventricular endocardium, which was consistent with the above results from the TGF-β-signal ligand-receptor interaction analysis (Figure 4F). Importantly, its expression was indeed rapidly downregulated in E14.5 and totally diminished by E16.5 (Figure 5F), as shown by both the percentage of TGFBR3-expressing cells (Figure 5G) and the expression intensity of TGFBR3 in individual cells (Figure 5H). We further examined the expression of *Twist1*, *Snail*, and *Snai2*, which encode important EMT transcription factors[30,32–34] and found that only SNAI2 was expressed in ventricular endocardial cells (Figures 5I, S5A, and S5B). Similarly, the percentage of SNAI2-expressing endocardial cells and the expression intensity of SNAI2 in individual ventricular endocardial cells were decreased from E12.5 to E16.5 (Figures 5J and 5K). In addition, the expression of other common EMT markers such as ACTA2, PDGFRB, and VIMENTIN (VIM) was decreased in ventricular endocardial cells from E12.5 to E16.5 (Figures S5C–S5K).

GO and KEGG pathway-enrichment analysis for the developmentally upregulated genes in cluster 0 from E12.5 to E15.5 showed that angiogenesis was a top enriched function, supported by upregulated expression of *Gata2* and *Tgfbr2* (Figures 5L and 5M). Expression of *Gata2*, a transcriptional factor essential for angiogenesis,[35] was examined by immunostaining. GATA binding protein 2 (GATA2) was expressed by some ventricular endocardial cells of E12.5 heart (Figure 5N), but the percentage of GATA2-expressing ventricular endocardial cells and the expression intensity of GATA2 in individual endocardial cells were significantly increased from E12.5 to E16.5 (Figures 5O and 5P). Furthermore, as NOTCH signaling is a well-known negative regulator of angiogenesis,[36–38] we examined the expression of NOTCH1 intracellular domain (NICD) and found that the percentage of NICD-expressing ventricular endocardial cells and the expression level of NICD in individual ventricular endocardial cell were significantly decreased from E12.5 to E16.5 (Figures 5Q–5S).

These observations demonstrate developmentally regulated functional changes in ventricular endocardial cells, especially downregulated EMT and upregulated angiogenesis that precede formation of trabecular vessels. Importantly, EMT by ventricular endocardial cells has not been recognized previously and is distinct from EMT by valve endocardial cells at E9.5–E11.5, which is critical for valvulogenesis.[39–42] Hence, we named EMT by ventricular endocardial cells at E12.5 angioEMT for its potential involvement in generating the angiogenic progenitor cells required for trabecular-vessel formation.

Ventricular endocardial cells form trabecular vessels by angioEMT

To test this angioEMT hypothesis, we performed an *ex vivo* coronary-sprouting assay using the left ventricle isolated from E12.5 heart (Figure 6A). The ventricular endocardial cells were labeled by GFP in Bmx^{CreER};$R26^{fsGFP}$ embryos induced by tamoxifen at E11.5. Bmx^{CreER} was used as it specifically labeled ventricular endocardial cells (Figure S6A). The left ventricle explants were cultured in a 3D Matrigel with or without recombinant TGFB2 treatment as ligand-receptor analysis suggested that only the TGFB2 ligand interacted with the TGFBR3 receptor expressed by ventricular endocardial cells (Figure 4G). We carried out both dose-dependent and time course experiments using recombinant TGFB2 at the concentration of 10 ng/mL for 1 day or 2 ng/mL for 3 days, and TGFB2 treatment

was followed by recombinant VEGFA treatment at 10 ng/mL (Figure 6A). GFP-labeled sprouting cells from ventricular endocardial cells and the formation of GFP-labeled vascular networks were examined at days 3, 6, and 9 after the TGFB2 treatment. The results showed that at day 3, few GFP-labeled sprouting cells emerged from control ventricular explants without TGFB2 treatment, while significant GFP-labeled sprouting cells arose from ventricular explants treated with TGFB2 at the 10 ng/mL concentration for one day or 2 ng/mL for 3 days (Figures 6B and 6C). Subsequent VEGFA treatment supported angiogenesis by GFP-labeled sprouting cells to form elaborate vascular networks from day 6 to day 9, whereas control explants generated few vascular branches upon VEGFA treatment (Figures 6B and 6D). This supports that TGFB2 primes ventricular endocardial cells for angiogenesis through EMT.

To determine if angioEMT is the priming mechanism involving TGF-β signaling, we examined the expression of TGFBR3 in ventricular endocardium of E12.5 hearts of *Snai2* germline null embryos,[43] as TGFBR3 and SNAI2 were both highly expressed in ventricular endocardial cells and developmentally downregulated from E12.5 to E15.5 (Figures 5F–5K). We found that TGFBR3 expression in ventricular endocardial cells was reduced in E12.5 *Snai2* null hearts (Figures S6B–S6D), suggesting that angioEMT by ventricular endocardial cells at E12.5 was regulated by SNAI2-TGFBR3 signaling. Trabecular vessels in P7 *Snai2* null hearts carrying *Npr3*^{CreERT2};*R26*^{fsGFP} were also examined. We found that P7 *Snai2* null hearts had a significantly reduction in GFP-labeled trabecular vessels derived from ventricular endocardial cells marked at E12.5 compared with control (wild-type) hearts (Figures S6E and S6F). Quantitative analysis showed that GFP-labeled trabecular-vessel density and the percentage of trabecular vessels in the left ventricle were significantly decreased (Figures S6G and S6H).

To exclude potential earlier EMT defects in *Snai2* nulls, which might complicate the trabecular-vessel phenotype and to link SNAI2-dependent angioEMT to TGF-β signaling, we applied the TGF-β inhibitor, SB431542,[44] to pregnant dams of *Npr3*^{CreERT2};*R26*^{fsGFP} on three consecutive days at E12.5, E13.5, and E14.5. The pregnant dams also had induced GFP labeling of ventricular endocardial cells by tamoxifen at E12.5. P7 hearts from pregnant dams treated with SB431542 had reduced formation of trabecular vessels by GFP-labeled progenies derived from E12.5 ventricular endocardial cells compared with P7 control hearts from PBS-treated pregnant dams (Figures S6I and S6J). Quantitative analysis confirmed that trabecular-vessel density and the percentage of trabecular vessels in the left ventricle were significantly decreased (Figures S6K and S6L).

Snai2 germline deletion or SB431542 treatment might inhibit the global EMT affecting multiple tissues or organs, thereby complicating the analysis of the specific trabecular-vessel phenotype. We thus overcame this limitation by specific deletion of *Tgfbr3* in the ventricular endocardium by crossing *Tgfbr3*-floxed mice[45] with *Npr3*^{CreERT2};*R26*^{fsGFP} mice. We induced *Tgfbr3* deletion at E12.5 when it was highly expressed in ventricular endocardial cells, some of which took the trabecular coronary fate. *Tgfbr3* deletion resulted in reduced trabecular vascular networks in P7 *Tgfbr3*^{cKO} heart compared with control hearts (Figures 6E and 6F). Quantitative analysis showed that trabecular-vessel density and the percentage of trabecular vessels in the left ventricle were significantly reduced (Figures 6G and 6H).

These observations from pharmacological and genetic studies demonstrate that angioEMT by ventricular endocardial cells is required for trabecular-vessel formation.

NOTCH1 regulates angiogenesis to form trabecular vessels

Our previous study showed that NOTCH1 signaling is required for the first-wave formation of coronary vessels at compact myocardium by ventricular endocardial cells through angiogenesis.[9] Therefore, we sought to determine if NOTCH1 signaling played a similar role in the second wave of coronary angiogenesis that gives rise to trabecular vessels. To this end, we overexpressed NICD to suppress angiogenesis by progenies of ventricular endocardial cells via crossing *R26*^{fsN1ICD} mice[46] with *Npr3*^{CreERT2} mice. We induced NICD overexpression at E12.5 in ventricular endocardial cells and their trabecular coronary endothelial progenies by tamoxifen and found that NICD overexpression inhibited the formation of trabecular vessels in P7 NICD heart compared with that in control hearts (Figures 7A and 7B). Quantitative analysis showed that trabecular-vessel density and the percentage of trabecular vessels in the left ventricle were significantly reduced (Figures 7C and 7D).

The overactivation of NOTCH1 signaling can suppress EMT by valve endocardial cells.[47,48] Therefore, we examined this possibility by studying the expression of TGFBR3 and found that its expression was not altered in the NICD-overexpressing ventricular endocardial cells at E13.5 (Figures S7A–S7C). Conversely, as SNAI2 might regulate NOTCH1 signaling to control EC activation and angiogenesis,[49] we examined NICD expression in *Snai2* null hearts and found that its expression remained at the same level in the *Snai2* null ventricular endocardial cells at E14.5 (Figures S7D–S7F). Together with the VEGFA findings (Figures 1 and S1), these observations support a sequential TGF-β and VEGFA-NOTCH1 signaling cascade that regulates angioEMT by ventricular endocardial cells and the subsequent second wave of coronary angiogenesis by the post-EMT ventricular endocardial cells to form trabecular vessels.

DISCUSSION

Trabecular myocardium of the left ventricle, located underneath the endocardium, is the most frequently damaged heart muscle by ischemia in coronary heart disease.[2] Hence, regeneration of trabecular vessels is inevitably needed to effectively relieve the ischemic insult to trabecular myocardium. However, little is known regarding how trabecular vessels are formed during development, which is essential for devising cell-type-specific strategies for the regeneration of trabecular vessels. In this study, we addressed this important knowledge gap and provided several lines of evidence demonstrating that trabecular vessels are derived from a subset of ventricular endocardial cells through a previously unrecognized angioEMT mechanism regulated by sequential SNAI2-TGFB2/TGFBR3 and VEGFA-NOTCH1 signaling.

First, we employed a time course lineage tracing strategy to precisely show that ventricular endocardial cells are the major embryonic source of trabecular vessels. In contrast, coronary vessels at compact myocardium are known to have three embryonic origins in the ventricular endocardium,[8–10,12] the sinus venous endothelium,[13] and the

proepicardium.[14,15] Specifically, our lineage tracing analysis clearly identified two distinct waves of developmental coronary vascularization in the ventricle wall by the angiogenic cells derived from ventricular endocardium. The first wave was characterized by a subset of ventricular endocardial cells labeled at E10.5 that gave rise to a significant portion of coronary vessels at compact myocardium of both ventricles, especially the left ventricle, at E16.5 when no vessels were present at trabecular myocardium. The second wave was defined by a subset of ventricular endocardial cells labeled at E12.5, which generated entire vessels at trabecular myocardium after E16.5 and did not contribute to new vessels at compact myocardium.

Second, our time course lineage tracing identified a developmentally regulated angiogenic potential for ventricular endocardial cells to become trabecular vessels from E12.5 to E16.5 and loss of potential by E16.5 (Figure 7E). During this developmental window, the progenitor cells were located within the ventricular endocardium and only underwent angiogenesis after E16.5 when trabecular myocardium became hypoxic (Figure 7E). Third, by scRNA-seq analysis and immunofluorescence validation, we found that decreased angiogenic potential was accompanied by decreased EMT and increased angiogenesis function in ventricular endocardial cells (Figure 7E). The two waves of coronary vascularization in this study are different from the previously described three waves of coronary angiogenesis, focused on angiogenic cells from different origins and/or locations.[50] Our study highlights definitively, for the first time, two waves of coronary vascularization by ventricular endocardial cells.

Lastly, we carried out *ex vivo* pharmacological treatment and *in vivo* loss- or gain-of-function genetic alteration to document a previously unknown “two-step” angioEMT mechanism. Ventricular endocardial cells first underwent EMT regulated by SNAI2-TGFB2/TGFBR3 signaling to become angiogenic fated progenitors for trabecular vessels and then were activated by VEGFA-NOTCH1 signaling to undergo the second wave of coronary angiogenesis to form trabecular vessels (Figure 7F). Interestingly, a recent study reported that BMP2, a key EMT regulator,[47,51] promotes the first wave of coronary angiogenesis by ventricular endocardial cells stimulated by VEGFA.[12] The synergistic functions of BMP2 and VEGFA during the first wave of coronary angiogenesis appear to be different from the two-step sequential functions of the SNAI2-TGFB2/TGFBR3 and VEGFA-NOTCH1 during the second wave of coronary angiogenesis.

Although the potential of ventricular endocardial cells to form coronary vessels is totally lost postnatally during normal development and neonatal heart regeneration[10] or is very limited after birth,[52] recent studies have demonstrated a phenomenon of formation of new trabecular vessels by ventricular endocardial cells in the injured adult heart overexpressing VEGFB in CMs[53] or VEGFR2 in ventricular endocardial cells.[54] These observations support the idea that adult ventricular endocardial cells may keep some potential to differentiate into coronary vascular ECs under certain genetically altered and/or pathological conditions. Our results advocate angioEMT as a potential therapeutic target to reactivate the potential of ventricular endocardial cells in the damaged adult heart to regenerate new trabecular vessels.

Limitations of the study

In this study, we did not test whether the developmental angioEMT program can be reactivated in ventricular endocardial cells in the adult heart—for example, after ischemic heart attack—to revascularize the diseased heart; this is a direction for further investigation. Future studies are also required to characterize the distinction between the earlier and later ventricular-endocardial-to-coronary-endothelial transition during the two waves of coronary angiogenesis.

STAR★METHODS

RESOURCE AVAILABILITY

Lead contact—Further information and requests for resources and reagents should be directed to the lead contact, Bin Zhou (bin.zhou@einsteinmed.edu).

Materials availability—The materials used and generated in this study are available from the lead contact upon reasonable request with a completed Materials Transfer Agreement.

Data and code availability—scRNA-seq data have been deposited at “GEO database:GSE205394”. Microscopy data reported in this paper will be shared by the lead contact upon request.

EXPERIMENTAL MODEL AND SUBJECT DETAILS

Mice—Mice were used in this study. Mouse housing and experiments were performed according to the protocol approved by the Institutional Animal Care and Use Committee (IACUC) of Albert Einstein College of Medicine. Mice were maintained under specific pathogen-free conditions in mouse rooms with a 12 h/12 h light/dark cycle at 22°C under ~55% humidity. Mice received sterile autoclaved water and a standard diet for rodents. Noontime on the day of detecting vaginal plugs was designated as E0.5, and morning on the day of observing newborns was designated as P0. For embryo generation, female mice at the age of ~4 months and male mice at the age of 3–6 months were used. Embryos were isolated and neonates were collected at different stages and inspected to determine expected developmental ages. Age-matched embryos and neonatal mice of both sexes were grouped according to genotype during experiments. The previous described *Vegfa*$^{f/f}$,[24] *Tnt*$^{\text{MerCreMer}}$,[23] *Npr3*^{CreERT2},[10] *R26*^{fsGFP},[56] *Bmx*$^{\text{CreER}}$,[55] *Snai2*$^{-/-}$,[43] *Tgfbr3*$^{f/f}$,[45] *R26*^{fsN1ICD}[46] mouse lines were used in this study.

METHOD DETAILS

All procedures were performed under protocols approved by the IACUC of Albert Einstein College of Medicine.

Lineage tracing analysis—The *Npr3*^{CreERT2} mice or *Bmx*$^{\text{CreER}}$ mice were bred with the *R26*^{fsGFP} reporter mice. Tamoxifen (100 mg/kg) was given to pregnant female mice by oral gavage to induce reporter gene expression. The *Npr3*^{CreERT2};*R26*^{fsGFP} mice were bred with the *Snai2*$^{-/-}$, *Tgfbr3*$^{f/f}$, *R26*^{fsN1ICD} mice to respectively induce reporter gene expression under gene deletion or overexpression background at a desired time point, and

wildtype littermates from the same dam which received tamoxifen (100 mg/kg) treatment as controls. The *Tnt*^{MerCreMer} mice were bred with the *Vegfa*$^{f/f}$ mice. The pregnant dams were given tamoxifen (100 mg/kg) by oral gavage to induce gene deletion at E17.5. Following induction, embryos or neonates from the same litter were sacrificed at indicated time points, and the hearts were isolated and analyzed in subsequent experiments.

Immunofluorescence staining—Preparation of paraffin sections and immunostaining were carried out as described.[10] Briefly, embryonic hearts were freshly isolated in PBS, fixed in 4% PFA at 4°C for 2 h to overnight according to developmental stages, washed in PBS, dehydrated through a serial of gradient ethanol, cleared in xylene and embedded in paraffin with orientation for front or transverse sections. The hearts were then sectioned at a 6μm thickness, and tissue sections were mounted on positive charged slides. The heart tissue sections were then baked overnight at 40°C and deparaffinized in xylene, rehydrated by a serial of gradient ethanol, and antigen retrieved before immunofluorescence staining. The tissue paraffin sections were blocked with 5% normal horse or goat serum for 1 h at room temperature and incubated with primary antibodies in blocking buffer at 4°C overnight. Then the tissues were incubated with secondary antibodies conjugated with the Alexa fluorescence dyes for 1 h at room temperature. Fluorescence micrographs were taken on a Zeiss Observer Z1 microscope or a Leica SP5 confocal microscope. Three to six hearts were analyzed for each genotype, and quantifications were carried out in a blinded fashion using the ImageJ 1.48v software.

Preparation of frozen sections and immunostaining were carried out as described.[10] Briefly, embryonic or neonatal hearts were freshly isolated in PBS, fixed in 4% PFA at 4°C for 1–3 h according to developmental stages, washed in PBS, soaked in 15% and 30% sucrose sequentially, and embedded in the optimal cutting temperature (OCT) compound with orientation for front or transverse sections. The hearts were then sectioned at an 8μm thickness, mounted on positive charged slides, post-fixed in 1:1 cold ethanol and acetone solution for 5 min and stored at −80°C. The heart tissue sections were air dried for 45 min before immunofluorescence staining. The frozen sections were blocked with 5% normal horse or goat serum for 1 h at room temperature and incubated with primary antibodies in blocking buffer at 4°C overnight. Then the tissues were incubated with secondary antibodies conjugated with the Alexa fluorescence dyes for 1 h at room temperature. Fluorescence micrographs were taken on a Zeiss Observer Z1 microscope or a Leica SP5 confocal microscope. Three to six hearts were analyzed for each genotype, and quantifications were carried out in a blinded fashion using the ImageJ 1.48v software.

Detection of myocardial hypoxia—Hypoxia in embryonic hearts was detected using Hypoxyprobe Kit (Hypoxyprobe Inc, HP1–100Kit). The pregnant female mice were injected with Hypoxyprobe^{TM-1} through intraperitoneal (IP) at a concentration of 60 mg/kg body weight. After 90 min pulse, the hearts were isolated and processed for frozen section as described above. The hypoxic tissue was then detected by immunofluorescence staining with Hypoxyprobe antibodies (1:100) in blocking buffer at 4 °C overnight and then donkey anti-mouse Alexa Fluor 488 (Thermo Fisher Scientific, A-21202, 1:200) secondary antibodies for 1 h in blocking buffer at room temperature. The stained heart tissues were photographed

using a Zeiss Observer Z1 microscope or a Leica SP5 confocal microscope. Three to six hearts were analyzed for each genotype. Quantifications were carried out in a blinded fashion using the ImageJ 1.48v software.

Left ventricular explant culture—Left ventricular explant culture was performed and adapted as previously described.[8] Hearts were isolated in cold PBS from E12.5 *Bmx*^{CreER}*;R26*^{fsGFP} embryos which were tamoxifen induced at E11.5. After removal of the atrium, the right ventricle, and septum of the heart, the left ventricle was rinsed with PBS twice to remove circulating cells, placed on the surface of pre-casted basement membrane matrix (200 μl/well) (BD Matrigel, growth factor reduced) in Nunc 4-well plates, and then sandwiched by adding an additional 150 μl of Matrigel. The Matrigel was prepared by addition of an equal volume of Endothelial Cell Growth Basal Medium (R&D, Cat# CCM029) with or without a testing growth factor, including Vegf120 (R&D, Cat# 494-VE-025) and Tgfb2 (R&D, Cat# 7346-B2–005). The final concentration of Vegf120 growth factor in the cultures was 10 ng/ml and Tgfb2 growth factor in the cultures was 2 ng/ml or 10 ng/ml, respectively. Heart explants were cultured at 37°C for up to nine days. The features of angiogenesis including transmural migration, sprouting, and endothelial networking were examined and photographed.

Antibodies—EMCN (Santa Cruz, sc-65495, 1:100), GFP (Abcam, ab6673, 1:500), PECAM1 (BD Pharmingen, 550274, 1:100), NPR3 (Santa Cruz, sc-515449, 1:100), IB4 (Sigma, L-2140, 1:50), VEGFR3 (R&D, AF743, 1:100), SNAI2 (Cell Signaling, 9585S, 1:100), TGFBR3 (R&D, AF242-PB, 1:100), GATA2 (R&D, AF2046, 1:100), and NICD (Cell Signaling, 4147S, 1:100) were used. The secondary antibodies used in the study included donkey anti-rat Alexa Fluor 488 (Thermo Fisher Scientific, A-21208, 1:200), donkey anti-rat Alexa Fluor 594 (Thermo Fisher Scientific, A-21209, 1:200), donkey anti-rabbit Alexa Fluor 488 (Thermo Fisher Scientific, A-21206, 1:200), donkey anti-rabbit Alexa Fluor 568 (Thermo Fisher Scientific, A-10042, 1:200), donkey anti-goat Alexa Fluor 488 (Thermo Fisher Scientific, A-11055, 1:200), donkey anti-goat Alexa Fluor 594 (Thermo Fisher Scientific, A-11058, 1:200), donkey anti-mouse Alexa Fluor 488 (Thermo Fisher Scientific, A-21202, 1:200), and Fluorescein Avidin DCS (Vector Laboratories, A-2011, 1:50).

Single-cell RNA-Seq protocol

Sample preparation: Two to five whole hearts from E12.5, E13.5, E14.5 and E15.5 were isolated in cold PBS and dissociated into single cells with 2mg/ml Papain (Brainbits) at 37 °C for about 2 to 5 min depending on the embryonic stage. Single cell suspensions were filtered through a 70um strainer. Single cells were washed in cold PBS and counted using a hemocytometer. 10,000 single cells in each sample were loaded onto the 10X Chromium Controller and cDNA libraries were prepared using the 10X Chromium Next GEM Single cell 3’ Kit v2 according to the manufacturer’s instruction (10X Genomics). The cDNA libraries were then sequenced by an Illumina NextSeq 500. Second duplicates for E13.5, E14.5 and E15.5 stage were obtained using the same method.

Processing and alignment of sequencing data: Raw scRNA-seq data was processed using the 10x Genomics CellRanger software, with default parameters and mapped to the mouse reference genome (GRCm38) (version 3.1.0).

Processing count data—Analysis of the scRNA-seq count data for each dataset was performed using the Seurat (v4.2.0) package in R.[57] Quality control filtering metrics were applied, by filtering out cells with less than 1,800 and greater than 6,000 detected genes. Additionally, cells with more than 30% of reads mapped to mitochondrial genes were filtered out. Counts were log-transformed and normalized, and highly variable genes were identified using default setting. The normalized data was scaled by linear transformation and dimensional reduction using principal component analysis (PCA) was conducted.

Integration of individual datasets—Integration anchors were determined using FindIntegrationAnchors (dims=1:25) in Seurat. The dataset was then integrated and scaled using IntegrateData() and ScaleData(), respectively. PCA was performed and Uniform Manifold Approximation and Projection (UMAP) dimensionality reduction was conducted using RunUMAP (dims=1:35). Cell clusters were determined by FindNeighbors (dims=1:35) and FindClusters() with a resolution of 1.5. Differential expression between clusters was performed to find cluster markers, and the cell type of each cluster was determined using known marker genes.

Re-clustering of endothelial cells—Clusters from the integrated dataset expressing pan-endothelial marker genes were taken. Data for the endothelial clusters was then scaled and PCA was performed. The k-nearest neighbors of each cell and clustering was performed by FindNeighbors (dims=1:35) and FindClusters() resolution of 0.1, respectively. T-distributed Stochastic Neighbor Embedding (tSNE) dimensionality reduction was conducted using RunTSNE (dims=1:25). Cell type of each cluster was determined by differential expression of marker genes.

Ligand-receptor interaction analysis: Cell–cell interactions were inferred by CellChat (v1.1).[26] The default mouse CellChat database was altered to include Tgfb2 - (Tgfbr2+Tgfbr3) as it was not included in the database. The default setting in CellChat was used to identify interaction for all cardiomyocyte clusters, coronary endothelial cluster and endocardium cluster 0 and 4.

Average expression: Plots showing average expression were generated by performing range standardization on the expression of each gene of interest. Data for genes in the same process were grouped for LOESS curve fitting and visualization of the data was generated with ggplot2 (v3.3.5).

Ordering cells along developmental trajectory: The endocardial cluster 0 and 4 and endothelial cluster 2 were subjected to trajectory inference using the DiffusionMap function of Destiny(v3.8.1).[58] Normalized log-counts of each cell were used as input to run DiffusionMap() and compute inferred diffusion component eigenvectors. Diffusion component eigenvectors were then ranked to calculate diffusion pseudotime (dpt). Cells

from Cluster 0, 2, and 4 were plotted along this expected differentiation trajectory in Figure 5A.

Differential expression analysis: Differentially expressed (DE) genes within cluster 0 were determined using edgeR (v3.36.0). DE genes were determined between stage E12 and each of the three later stages, E13, E14, and E15. The smallest p-value from the three comparisons was used with an adjusted p-value < 0.01 for significance. Differentially expressed genes (DEGs) between cluster 0 and cluster 4 were determined by FindMarkers() with parameters such that positive avg_log2FC indicates genes upregulated in cluster 4.

Gene ontology enrichment analysis: Gene set enrichment analysis was performed with the clusterProfiler (v 4.2.2) package using q < 0.05 as a cutoff. Similar gene ontology (GO) terms were grouped to simplify redundant functions with rrvgo (v.1.6.0).

QUANTIFICATION AND STATISTICAL ANALYSIS

Statistics and reproducibility—No statistical methods were used to predetermine sample size. Student's t-test (two-tailed) was used for statistical difference between groups, assuming unequal variance from three to six samples (i.e., hearts) in independent experiments. Numbers of animals used are described in the corresponding figure legends. Normality was assumed and variance was compared between groups. Sample size was determined based upon previous experience in the relevant experiments described previously. The investigators were not blinded to the group allocation during experiments, but the outcome assessment was blinded. All numerical data were presented as mean ± SD and P value of <0.05 was considered as significant.

Supplementary Material

Refer to Web version on PubMed Central for supplementary material.

ACKNOWLEDGMENTS

We thank Prof. Ralf H. Adams for sharing the *Bmx*^{CreER} mouse line. This work was supported by grants from the American Heart Association (AHA-17POST33410599 to P.L.) and the National Heart Lung and Blood Institute (NHLBI) of the United States (HL133120, HL148128, HL157347, and HD092944 to B.Z. and D.Z.).

REFERENCES

1. Hoffman JI, and Buckberg GD (1975). Pathophysiology of subendocardial ischaemia. Br. Med. J. 1, 76–79. 10.1136/bmj.1.5949.76. [PubMed: 1109663]
2. Captur G, Wilson R, Bennett MF, Luxán G, Nasis A, de la Pompa JL, Moon JC, and Mohun TJ (2016). Morphogenesis of myocardial trabeculae in the mouse embryo. J. Anat. 229, 314–325. 10.1111/joa.12465. [PubMed: 27020702]
3. Del Monte-Nieto G, Ramialison M, Adam AAS, Wu B, Aharonov A, D'Uva G, Bourke LM, Pitulescu ME, Chen H, de la Pompa JL, et al. (2018). Control of cardiac jelly dynamics by NOTCH1 and NRG1 defines the building plan for trabeculation. Nature 557, 439–445. 10.1038/s41586-018-0110-6. [PubMed: 29743679]
4. Townsend N, Nichols M, Scarborough P, and Rayner M (2015). Cardiovascular disease in Europe—epidemiological update 2015. Eur. Heart J. 36, 2696–2705. [PubMed: 26306399]

5. Mozaffarian D, Benjamin EJ, Go AS, Arnett DK, Blaha MJ, Cushman M, de Ferranti S, Després JP, Fullerton HJ, Howard VJ, et al. (2015). Heart disease and stroke statistics–2015 update: a report from the American Heart Association. Circulation 131, e29–e322. 10.1161/CIR.0000000000000152. [PubMed: 25520374]
6. Ylä-Herttuala S, Bridges C, Katz MG, and Korpisalo P (2017). Angiogenic gene therapy in cardiovascular diseases: dream or vision? Eur. Heart J. 38, 1365–1371. 10.1093/eurheartj/ehw547. [PubMed: 28073865]
7. Dragneva G, Korpisalo P, and Ylä-Herttuala S (2013). Promoting blood vessel growth in ischemic diseases: challenges in translating preclinical potential into clinical success. Dis. Model. Mech. 6, 312–322. [PubMed: 23471910]
8. Wu B, Zhang Z, Lui W, Chen X, Wang Y, Chamberlain AA, Moreno-Rodriguez RA, Markwald RR, O'Rourke BP, Sharp DJ, et al. (2012). Endocardial cells form the coronary arteries by angiogenesis through myocardial-endocardial VEGF signaling. Cell 151, 1083–1096. 10.1016/j.cell.2012.10.023. [PubMed: 23178125]
9. Wang Y, Wu B, Lu P, Zhang D, Wu B, Varshney S, del Monte-Nieto G, Zhuang Z, Charafeddine R, Kramer AH, et al. (2017). Uncontrolled angiogenic precursor expansion causes coronary artery anomalies in mice lacking Pofut1. Nat. Commun. 8, 578. [PubMed: 28924218]
10. Lu P, Wang Y, Liu Y, Wang Y, Wu B, Zheng D, Harvey RP, and Zhou B (2021). Perinatal angiogenesis from pre-existing coronary vessels via DLL4-NOTCH1 signalling. Nat. Cell Biol. 23, 967–977. 10.1038/s41556-021-00747-1. [PubMed: 34497373]
11. Sharma B, Ho L, Ford GH, Chen HI, Goldstone AB, Woo YJ, Quertermous T, Reversade B, and Red-Horse K (2017). Alternative progenitor cells compensate to rebuild the coronary vasculature in Elabela- and Apj-deficient hearts. Dev. Cell 42. 655–666.e3. 10.1016/j.devcel.2017.08.008. [PubMed: 28890073]
12. D'Amato G, Phansalkar R, Naftaly JA, Fan X, Amir ZA, Rios Coronado PE, Cowley DO, Quinn KE, Sharma B, Caron KM, et al. (2022). Endocardium-to-coronary artery differentiation during heart development and regeneration involves sequential roles of Bmp2 and CXCL12/Cxcr4. Dev. Cell 57. 2517–2532.e6. 10.1016/j.devcel.2022.10.007. [PubMed: 36347256]
13. Red-Horse K, Ueno H, Weissman IL, and Krasnow MA (2010). Coronary arteries form by developmental reprogramming of venous cells. Nature 464, 549–553. 10.1038/nature08873. [PubMed: 20336138]
14. Pérez-Pomares JM, Carmona R, González-Iriarte M, Atencia G, Wessels A, and Muñoz-Chápuli R (2002). Origin of coronary endothelial cells from epicardial mesothelium in avian embryos. Int. J. Dev. Biol. 46, 1005–1013. [PubMed: 12533024]
15. Katz TC, Singh MK, Degenhardt K, Rivera-Feliciano J, Johnson RL, Epstein JA, and Tabin CJ (2012). Distinct compartments of the proepicardial organ give rise to coronary vascular endothelial cells. Dev. Cell 22, 639–650. [PubMed: 22421048]
16. Zhang Z, and Zhou B (2013). Accelerated coronary angiogenesis by vegfr1-knockout endocardial cells. PLoS One 8, e70570. 10.1371/journal.pone.0070570. [PubMed: 23894673]
17. Chen HI, Sharma B, Akerberg BN, Numi HJ, Kivelä R, Saharinen P, Aghajanian H, McKay AS, Bogard PE, Chang AH, et al. (2014). The sinus venosus contributes to coronary vasculature through VEGFC-stimulated angiogenesis. Development 141, 4500–4512. 10.1242/dev.113639. [PubMed: 25377552]
18. Cano E, Carmona R, Ruiz-Villalba A, Rojas A, Chau YY, Wagner KD, Wagner N, Hastie ND, Muñoz-Chápuli R, and Pérez-Pomares JM (2016). Extracardiac septum transversum/proepicardial endothelial cells pattern embryonic coronary arterio-venous connections. Proc. Natl. Acad. Sci. USA 113, 656–661. 10.1073/pnas.1509834113. [PubMed: 26739565]
19. Tomanek RJ, Ishii Y, Holifield JS, Sjogren CL, Hansen HK, and Mikawa T (2006). VEGF family members regulate myocardial tubulogenesis and coronary artery formation in the embryo. Circ. Res. 98, 947–953. 10.1161/01.RES.0000216974.75994.da. [PubMed: 16527987]
20. Pugh CW, and Ratcliffe PJ (2003). Regulation of angiogenesis by hypoxia: role of the HIF system. Nat. Med. 9, 677–684. [PubMed: 12778166]
21. Giordano FJ, Gerber HP, Williams SP, VanBruggen N, Bunting S, Ruiz-Lozano P, Gu Y, Nath AK, Huang Y, Hickey R, et al. (2001). A cardiac myocyte vascular endothelial growth factor paracrine

pathway is required to maintain cardiac function. Proc. Natl. Acad. Sci. USA 98, 5780–5785. 10.1073/pnas.091415198. [PubMed: 11331753]

22. Cousins FL, Murray AA, Scanlon JP, and Saunders PT (2016). Hypoxyprobe™ reveals dynamic spatial and temporal changes in hypoxia in a mouse model of endometrial breakdown and repair. BMC Res. Notes 9, 30. [PubMed: 26780953]
23. Yan J, Sultana N, Zhang L, Park DS, Shekhar A, Hu J, Bu L, and Cai CL (2015). Generation of a tamoxifen inducible Tnnt2MerCreMer knock-in mouse model for cardiac studies. Genesis 53, 377–386. 10.1002/dvg.22861. [PubMed: 26010701]
24. Gerber HP, Hillan KJ, Ryan AM, Kowalski J, Keller GA, Rangell L, Wright BD, Radtke F, Aguet M, and Ferrara N (1999). VEGF is required for growth and survival in neonatal mice. Development 126, 1149–1159. 10.1242/dev.126.6.1149. [PubMed: 10021335]
25. Cai CL, Martin JC, Sun Y, Cui L, Wang L, Ouyang K, Yang L, Bu L, Liang X, Zhang X, et al. (2008). A myocardial lineage derives from Tbx18 epicardial cells. Nature 454, 104–108. [PubMed: 18480752]
26. Jin S, Guerrero-Juarez CF, Zhang L, Chang I, Ramos R, Kuan CH, Myung P, Plikus MV, and Nie Q (2021). Inference and analysis of cell-cell communication using CellChat. Nat. Commun. 12, 1088. 10.1038/s41467-021-21246-9. [PubMed: 33597522]
27. Cai X, Zhang W, Hu J, Zhang L, Sultana N, Wu B, Cai W, Zhou B, and Cai CL (2013). Tbx20 acts upstream of Wnt signaling to regulate endocardial cushion formation and valve remodeling during mouse cardiogenesis. Development 140, 3176–3187. 10.1242/dev.092502. [PubMed: 23824573]
28. Marino N, Marshall JC, Collins JW, Zhou M, Qian Y, Veenstra T, and Steeg PS (2013). Nm23-h1 binds to gelsolin and inactivates its actin-severing capacity to promote tumor cell motility and metastasis. Cancer Res. 73, 5949–5962. 10.1158/0008-5472.CAN-13-0368. [PubMed: 23940300]
29. Akiyama H, Chaboissier MC, Behringer RR, Rowitch DH, Schedl A, Epstein JA, and de Crombrugghe B (2004). Essential role of Sox9 in the pathway that controls formation of cardiac valves and septa. Proc. Natl. Acad. Sci. USA 101, 6502–6507. 10.1073/pnas.0401711101. [PubMed: 15096597]
30. Yang J, Mani SA, Donaher JL, Ramaswamy S, Itzykson RA, Come C, Savagner P, Gitelman I, Richardson A, and Weinberg RA (2004). Twist, a master regulator of morphogenesis, plays an essential role in tumor metastasis. Cell 117, 927–939. 10.1016/j.cell.2004.06.006. [PubMed: 15210113]
31. Compton LA, Potash DA, Brown CB, and Barnett JV (2007). Coronary vessel development is dependent on the type III transforming growth factor beta receptor. Circ. Res. 101, 784–791. 10.1161/CIRCRESAHA.107.152082. [PubMed: 17704211]
32. Batlle E, Sancho E, Francí C, Domínguez D, Monfar M, Baulida J, and García de Herreros A (2000). The transcription factor snail is a repressor of E-cadherin gene expression in epithelial tumour cells. Nat. Cell Biol. 2, 84–89. [PubMed: 10655587]
33. Cano A, Pérez-Moreno MA, Rodrigo I, Locascio A, Blanco MJ, del Barrio MG, Portillo F, and Nieto MA (2000). The transcription factor snail controls epithelial–mesenchymal transitions by repressing E-cadherin expression. Nat. Cell Biol. 2, 76–83. [PubMed: 10655586]
34. Hajra KM, Chen DY, and Fearon ER (2002). The SLUG zinc-finger protein represses E-cadherin in breast cancer. Cancer Res. 62, 1613–1618. [PubMed: 11912130]
35. Mammoto A, Connor KM, Mammoto T, Yung CW, Huh D, Aderman CM, Mostoslavsky G, Smith LE, and Ingber DE (2009). A mechanosensitive transcriptional mechanism that controls angiogenesis. Nature 457, 1103–1108. 10.1038/nature07765. [PubMed: 19242469]
36. Benedito R, Roca C, Sörensen I, Adams S, Gossler A, Fruttiger M, and Adams RH (2009). The notch ligands Dll4 and Jagged1 have opposing effects on angiogenesis. Cell 137, 1124–1135. 10.1016/j.cell.2009.03.025. [PubMed: 19524514]
37. Pitulescu ME, Schmidt I, Giaimo BD, Antoine T, Berkenfeld F, Ferrante F, Park H, Ehling M, Biljes D, Rocha SF, et al. (2017). Dll4 and Notch signalling couples sprouting angiogenesis and artery formation. Nat. Cell Biol. 19, 915–927. 10.1038/ncb3555. [PubMed: 28714968]
38. Hellström M, Phng LK, Hofmann JJ, Wallgard E, Coultas L, Lindblom P, Alva J, Nilsson AK, Karlsson L, Gaiano N, et al. (2007). Dll4 signalling through Notch1 regulates formation of tip cells during angiogenesis. Nature 445, 776–780. 10.1038/nature05571. [PubMed: 17259973]

39. Wu B, Wang Y, Lui W, Langworthy M, Tompkins KL, Hatzopoulos AK, Baldwin HS, and Zhou B (2011). Nfatc1 coordinates valve endocardial cell lineage development required for heart valve formation. Circ. Res. 109, 183–192. 10.1161/CIRCRESAHA.111.245035. [PubMed: 21597012]
40. Wu B, Wang Y, Xiao F, Butcher JT, Yutzey KE, and Zhou B (2017). Developmental mechanisms of aortic valve malformation and disease. Annu. Rev. Physiol. 79, 21–41. 10.1146/annurev-physiol-022516-034001. [PubMed: 27959615]
41. Eisenberg LM, and Markwald RR (1995). Molecular regulation of atrioventricular valvuloseptal morphogenesis. Circ. Res. 77, 1–6. 10.1161/01.res.77.1.1. [PubMed: 7788867]
42. de Lange FJ, Moorman AF, Anderson RH, Männer J, Soufan AT, de Gier-de Vries C, Schneider MD, Webb S, van den Hoff MJ, and Christoffels VM (2004). Lineage and morphogenetic analysis of the cardiac valves. Circ. Res. 95, 645–654. 10.1161/01.RES.0000141429.13560.cb. [PubMed: 15297379]
43. Jiang R, Lan Y, Norton CR, Sundberg JP, and Gridley T (1998). The Slug gene is not essential for mesoderm or neural crest development in mice. Dev. Biol. 198, 277–285. [PubMed: 9659933]
44. Inman GJ, Nicolás FJ, Callahan JF, Harling JD, Gaster LM, Reith AD, Laping NJ, and Hill CS (2002). SB-431542 is a potent and specific inhibitor of transforming growth factor-beta superfamily type I activin receptor-like kinase (ALK) receptors ALK4, ALK5, and ALK7. Mol. Pharmacol. 62, 65–74. 10.1124/mol.62.1.65. [PubMed: 12065756]
45. Li Y, Fortin J, Ongaro L, Zhou X, Boehm U, Schneyer A, Bernard DJ, and Lin HY (2018). Betaglycan (TGFBR3) functions as an inhibin A, but not inhibin B, coreceptor in pituitary gonadotrope cells in mice. Endocrinology 159, 4077–4091. 10.1210/en.2018-00770. [PubMed: 30364975]
46. Murtaugh LC, Stanger BZ, Kwan KM, and Melton DA (2003). Notch signaling controls multiple steps of pancreatic differentiation. Proc. Natl. Acad. Sci. USA 100, 14920–14925. 10.1073/pnas.2436557100. [PubMed: 14657333]
47. Luna-Zurita L, Prados B, Grego-Bessa J, Luxán G, Del Monte G, Benguría A, Adams RH, Pérez-Pomares JM, and De La Pompa JL (2010). Integration of a Notch-dependent mesenchymal gene program and Bmp2-driven cell invasiveness regulates murine cardiac valve formation. J. Clin. Invest. 120, 3493–3507. [PubMed: 20890042]
48. Timmerman LA, Grego-Bessa J, Raya A, Bertrán E, Pérez-Pomares JM, Díez J, Aranda S, Palomo S, McCormick F, Izpisúa-Belmonte JC, et al. (2004). Notch promotes epithelial-mesenchymal transition during cardiac development and oncogenic transformation. Genes Dev. 18, 99–115. 10.1101/gad.276304. [PubMed: 14701881]
49. Hultgren NW, Fang JS, Ziegler ME, Ramirez RN, Phan DTT, Hatch MMS, Welch-Reardon KM, Paniagua AE, Kim LS, Shon NN, et al. (2020). Slug regulates the Dll4-Notch-VEGFR2 axis to control endothelial cell activation and angiogenesis. Nat. Commun. 11, 5400. 10.1038/s41467-020-18633-z. [PubMed: 33106502]
50. Tian X, Hu T, Zhang H, He L, Huang X, Liu Q, Yu W, He L, Yang Z, Yan Y, et al. (2014). Vessel formation. De novo formation of a distinct coronary vascular population in neonatal heart. Science 345, 90–94. 10.1126/science.1251487. [PubMed: 24994653]
51. Ma L, Lu MF, Schwartz RJ, and Martin JF (2005). Bmp2 is essential for cardiac cushion epithelial-mesenchymal transition and myocardial patterning. Development 132, 5601–5611. 10.1242/dev.02156. [PubMed: 16314491]
52. Tang J, Zhang H, He L, Huang X, Li Y, Pu W, Yu W, Zhang L, Cai D, Lui KO, and Zhou B (2018). Genetic fate mapping defines the vascular potential of endocardial cells in the adult heart. Circ. Res. 122, 984–993. 10.1161/CIRCRESAHA.117.312354. [PubMed: 29374073]
53. Räsänen M, Sultan I, Paech J, Hemanthakumar KA, Yu W, He L, Tang J, Sun Y, Hlushchuk R, Huan X, et al. (2021). VEGF-B promotes endocardium-derived coronary vessel development and cardiac regeneration. Circulation 143, 65–77. 10.1161/CIRCULATIONAHA.120.050635. [PubMed: 33203221]
54. Jiang Z, Lu Z, Kou S, Feng T, Wei Y, Gao Z, Deng D, Meng J, Lin CP, Zhou B, and Zhang H (2021). Overexpression of Kdr in adult endocardium induces endocardial neovascularization and improves heart function after myocardial infarction. Cell Res. 31, 485–487. 10.1038/s41422-020-00436-y. [PubMed: 33219343]

55. Ehling M, Adams S, Benedito R, and Adams RH (2013). Notch controls retinal blood vessel maturation and quiescence. Development 140, 3051–3061. 10.1242/dev.093351. [PubMed: 23785053]

56. Miyoshi G, Hjerling-Leffler J, Karayannis T, Sousa VH, Butt SJ, Battiste J, Johnson JE, Machold RP, and Fishell G (2010). Genetic fate mapping reveals that the caudal ganglionic eminence produces a large and diverse population of superficial cortical interneurons. J. Neurosci. 30, 1582–1594. 10.1523/JNEUROSCI.4515-09.2010. [PubMed: 20130169]

57. Butler A, Hoffman P, Smibert P, Papalexi E, and Satija R (2018). Integrating single-cell transcriptomic data across different conditions, technologies, and species. Nat. Biotechnol. 36, 411–420. 10.1038/nbt.4096. [PubMed: 29608179]

58. Angerer P, Haghverdi L, Büttner M, Theis FJ, Marr C, and Buettner F (2016). destiny: diffusion maps for large-scale single-cell data in R. Bioinformatics 32, 1241–1243. 10.1093/bioinformatics/btv715. [PubMed: 26668002]

Highlights

- Trabecular coronary vessels arise from ventricular endocardial cells
- Trabecular coronary vessels are formed by a two-step angioEMT mechanism
- TGF-β signaling regulates the endocardial-coronary endothelial fate change via endocardial-mesenchymal transition
- VEGFA-NOTCH1 signaling drives trabecular coronary-vessel formation by angiogenesis

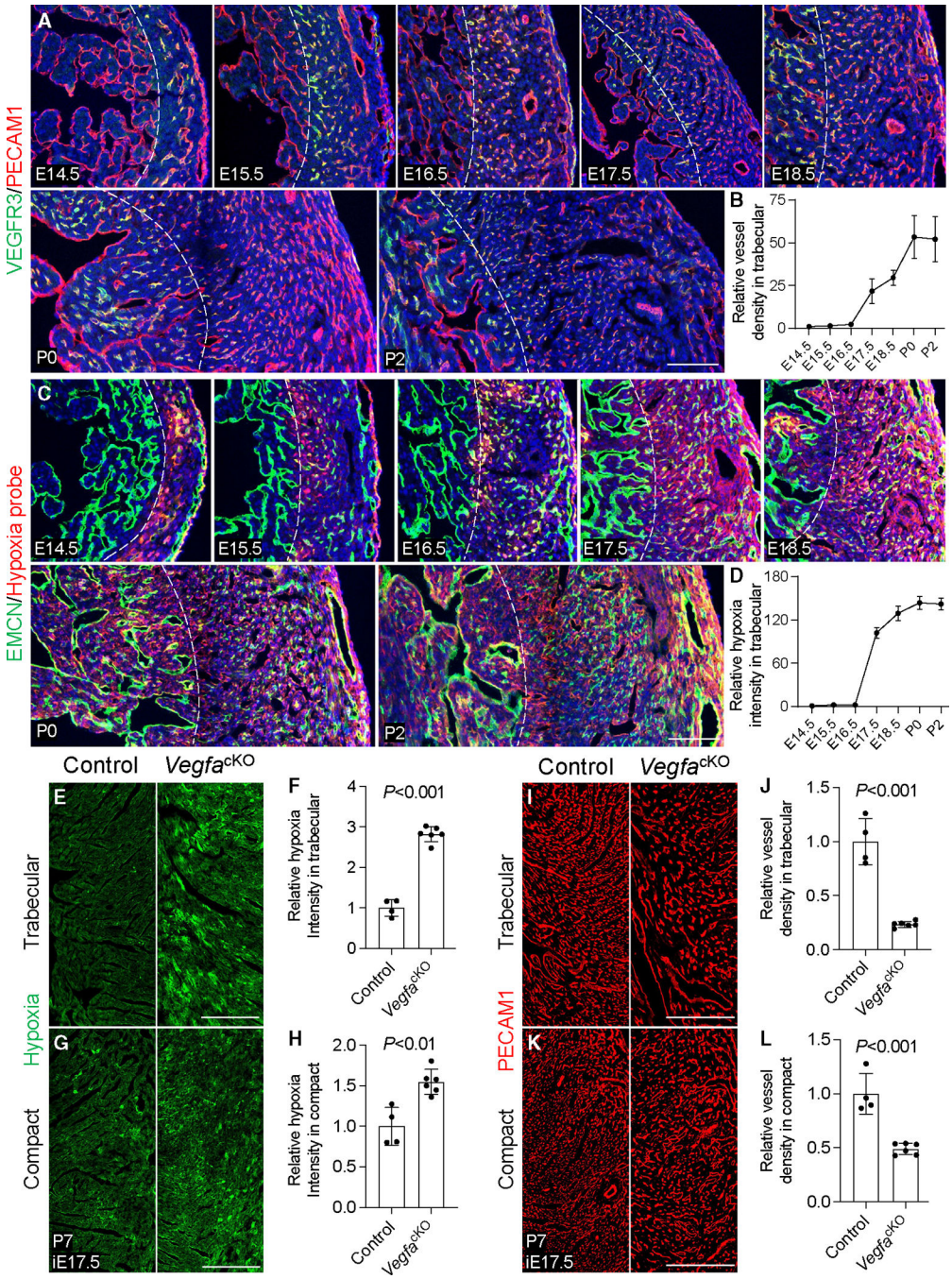

Figure 1. Myocardial *Vegfa* is required for trabecular-vessel formation

(A and B) Immunofluorescence (IF) shows increased density of (A) PECAM1-expressing (red) and (B) VEGFR3-expressing (green) coronary vessels at trabecular myocardium from E14.5 to P2 (n = 4 hearts for each stage. Dashed line separates trabecular and compact myocardium).

(C and D) IF shows increased hypoxia signaling intensity (red) at trabecular myocardium from E14.5 to P2. EMCN (green) labels ventricular endocardium (n = 5 hearts for each stage. Dashed line separates trabecular from compact myocardium).

(E–H) IF shows greater increase in the hypoxia signaling intensity (green) at trabecular myocardium (E and F) compared with the hypoxia intensity at compact myocardium (G and H) of P7 heart after inducing myocardial *Vegfa* deletion (*Vegfa*^{cKO}) at E17.5 (iE17.5) (n = 4 hearts for control and n = 6 hearts for *Vegfa*^{cKO}).

(I–L) IF shows greater decrease in the density of PECAM1-expressing coronary vessels (red) at trabecular myocardium (I and J) compared with the density of coronary vessels at compact myocardium (K and L) of P7 heart after inducing myocardial *Vegfa* deletion (*Vegfa*^{cKO}) at E17.5 (iE17.5) (n = 4 hearts for control; n = 6 hearts for *Vegfa*^{cKO}).

Scale bars: 100 μm. Error bars: SD. Statistical analysis was performed using two-tailed unpaired Student's t tests. See also Figure S1.

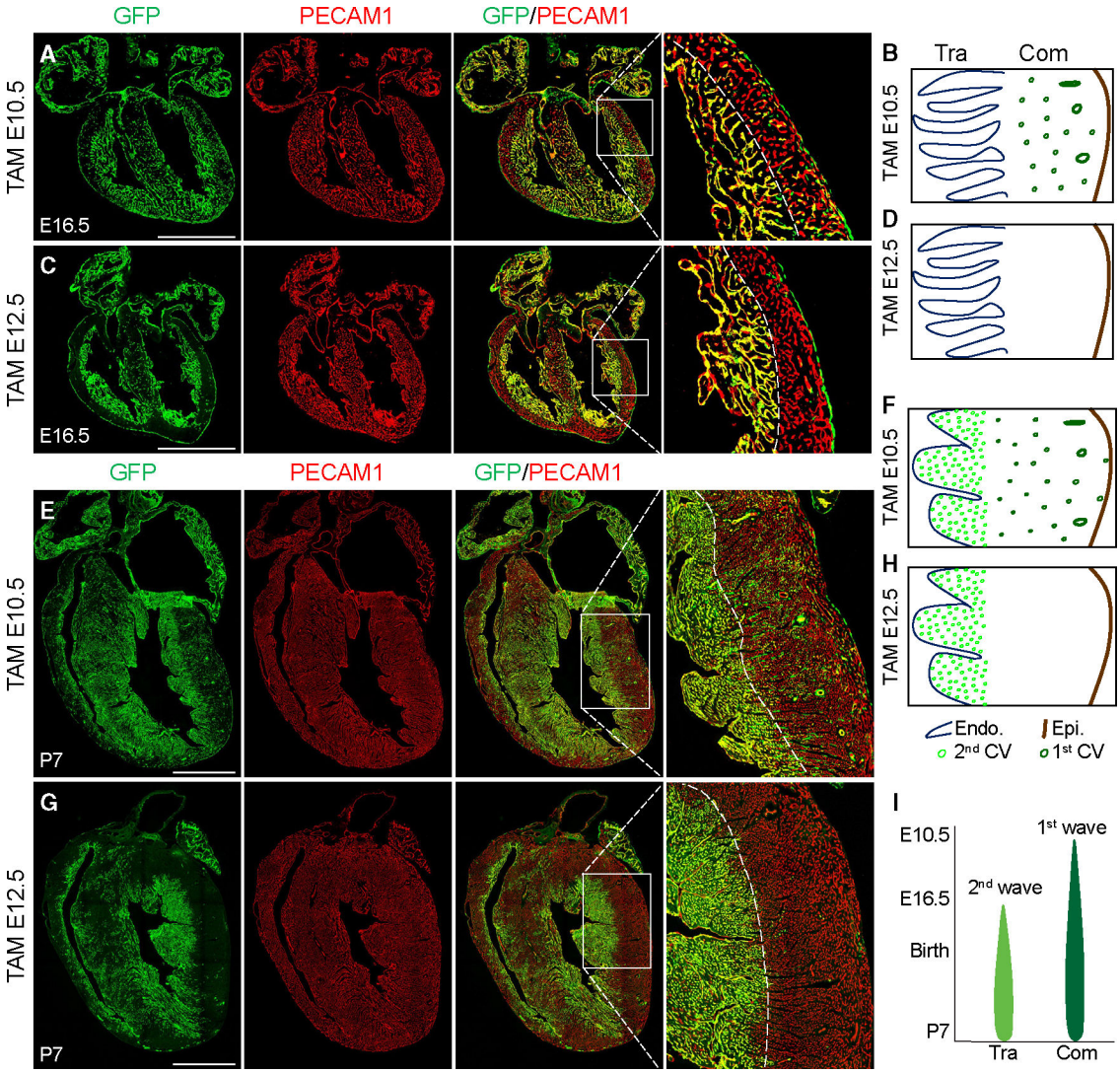

Figure 2. Ventricular endocardial cells give rise to trabecular vessels

(A) IF for PECAM1 (red) and GFP (green) shows GFP-labeled progenies derived from E10.5 (iE10.5) ventricular endocardial cells in ventricular endocardium and PECAM1-expressing coronary vessels at the left and right (to a lesser degree) ventricular wall and interventricular septum of E16.5 heart.

(B) Schematic shows GFP-labeled coronary vessels derived from E10.5 ventricular endocardial cells in the left ventricle of the E16.5 heart.

(C) IF for PECAM1 (red) and (green) shows GFP-labeled progenies derived from E12.5 (iE12.5) ventricular endocardial cells in ventricular endocardium of E16.5 heart, but not the PECAM1-expressing coronary vessels at both ventricular walls.

(D) Schematic shows the absence of GFP-labeled coronary vessels derived from E12.5 ventricular endocardial cells in the left ventricle of E16.5 heart.

(E) IF for PECAM1 (red) and GFP (green) shows GFP-labeled progenies derived from E10.5 (iE10.5) ventricular endocardial cells in ventricular endocardium, coronary vessels at both ventricular walls, and interventricular septum of P7 heart.

(F) Schematic shows the presence of GFP-labeled coronary vessels derived from E10.5 ventricular endocardial cells at trabecular and compact myocardium of P7 left ventricle.
(G) IF for PECAM1 (red) and GFP (green) shows the presence of GFP-labeled trabecular vessels derived from E12.5 (iE12.5) ventricular endocardial cells at both ventricular walls of P7 heart.
(H) Schematic shows GFP-labeled coronary vessels derived from E12.5 ventricular endocardial cells at trabecular but not at compact myocardium of P7 left ventricle.
(I) Schematic of two waves of coronary-vessel formation at the left ventricular wall by ventricular endocardial cells.
Scale bars: 1,000 μm. Dashed line separates trabecular myocardium (Tra) from compact myocardium (Com). (A), (C), (E), and (G) are representative of three individual hearts for each staining. See also Figure S2.

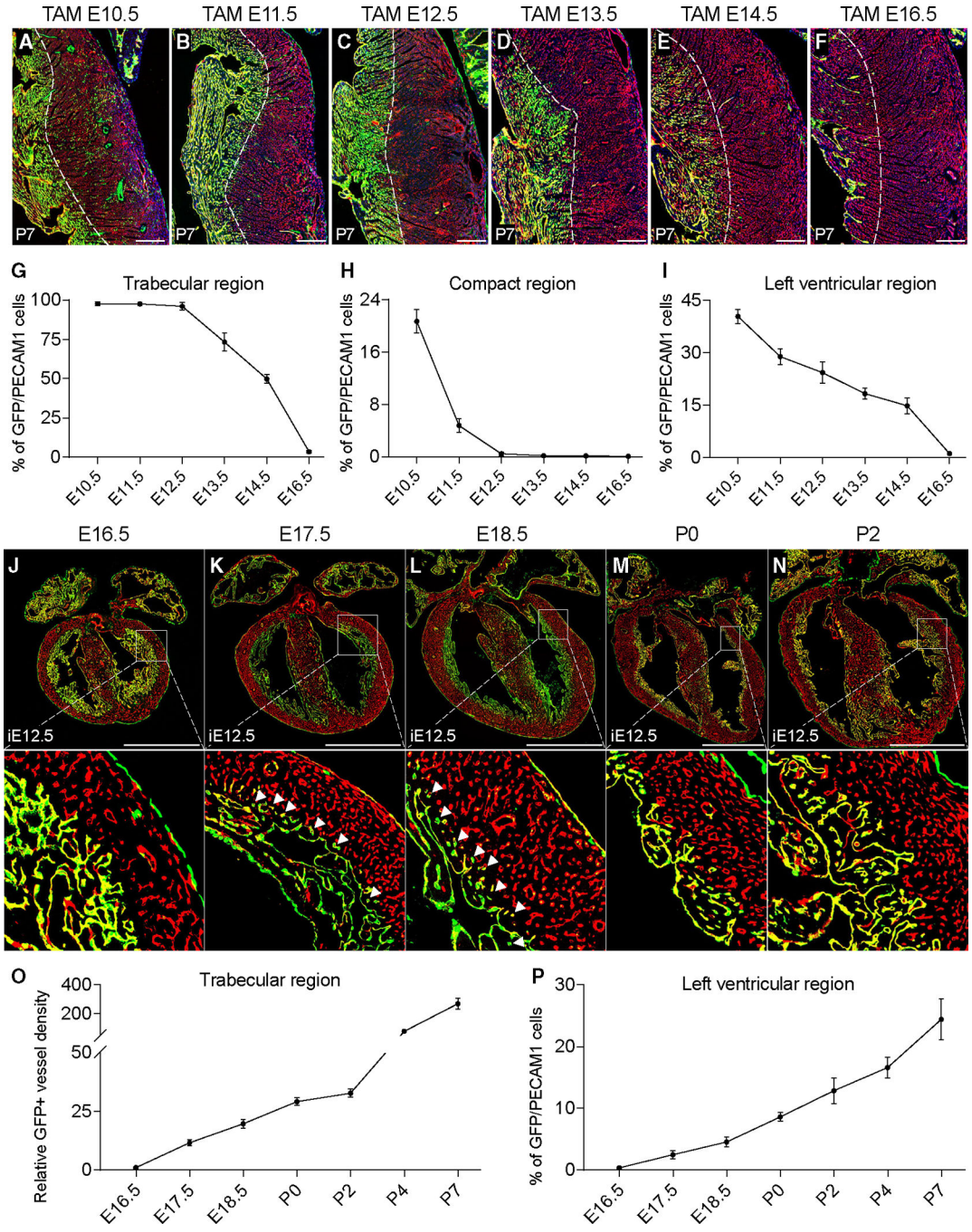

Figure 3. Characterization of second-wave coronary-vessel formation by ventricular endocardial cells through time course lineage analysis

(A–F) IF for PECAM1 (red), GFP (green), and DAPI (blue) shows GFP-labeled coronary vessels derived from E10.5 (A), E11.5 (B), E12.5 (C), E13.5 (D), E14.5 (E), or E16.5 (F) ventricular endocardial cells in P7 left ventricle. Dashed line separates trabecular and compact myocardium.

(G–I) Quantitative analysis of the percentage of GPF-expressing/PECAM1-expressing coronary vessels at trabecular (G), compact myocardium (H) and entire left ventricular wall (I) (n = 4 hearts for TAM at E10.5; n = 5 hearts for all other stages).

(J–N) IF for PECAM1 (red) and GFP (green) shows GFP-labeled coronary vessels derived from E12.5 (iE12.5) ventricular endocardial cells at trabecular myocardium of E16.5 (J), E17.5 (K, arrowheads), E18.5 (L, arrowheads), P0 (M), or P2 (N) heart.

(O and P) Quantitative analysis shows the relative density of GPF-expressing and PECAM1-expressing coronary vessels at trabecular myocardium (O) and the percentage of GPF-expressing/PECAM1-expressing coronary vessels at the left ventricle (P) (n = 4 hearts for each stage).

Scale bars: 200 μm for (A–F); 1,000 μm for (J–N). Error bars: SD. Statistical analysis was performed using two-tailed unpaired Student's t tests. See also Figure S3.

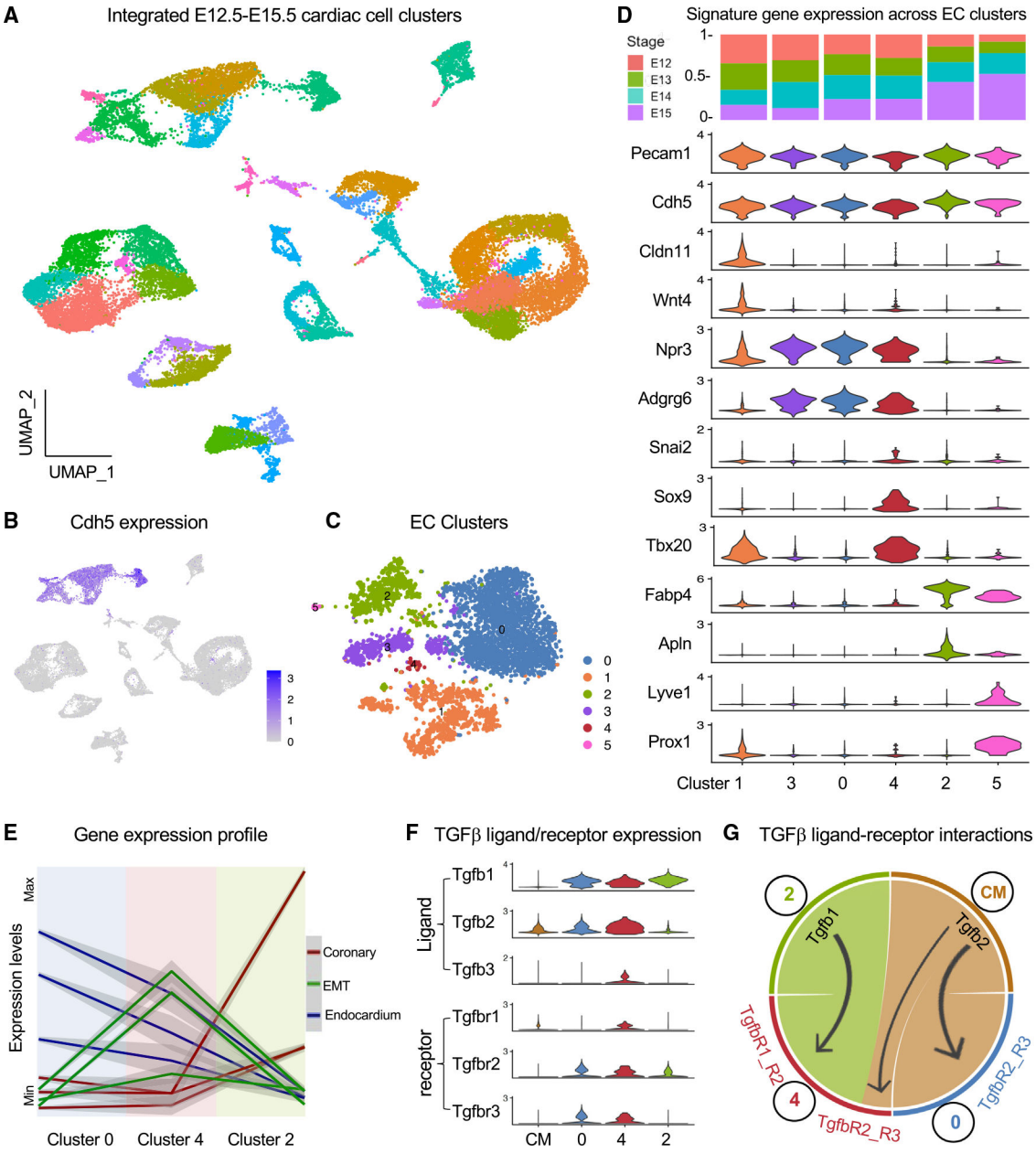

Figure 4. Characterization of ventricular endocardial and coronary endothelial cells

(A) Uniform manifold approximation and projection (UMAP) plot shows 38 clusters identified from the integrative and clustering analysis of single cells from E12.5, E13.5, E14.5, and E15.5 hearts. Duplications were performed for E13.5, E14.5, and E15.5 hearts.

(B) Feature plot highlights endothelial/endocardial cells, as marked by strong expression of endothelial marker *Cdh5*.

(C) t-distributed stochastic neighbor embedding (tSNE) plot shows six endothelial/endocardial cell (EC) clusters.

(D) Violin plots show the expression of the top maker genes in individual EC clusters.

(E) Standardized average expression profiles of genes in the three functional groups in two endocardial cell clusters (clusters 0 and 4) and one coronary endothelial cell cluster (cluster 2). Cluster 4 is featured with highly expressed EMT genes.
(F) Violin plots show the expression of genes encoding TGF-β ligands and receptors in cardiomyocytes (CMs), endocardial cells (clusters 0 and 4) and coronary vessels (cluster 2).
(G) Chord plot shows TGF-β ligand-receptor interactions among cardiomyocytes (CM), endocardial cells (clusters 0 and 4), and coronary vessels (cluster 2). See also Figure S4.

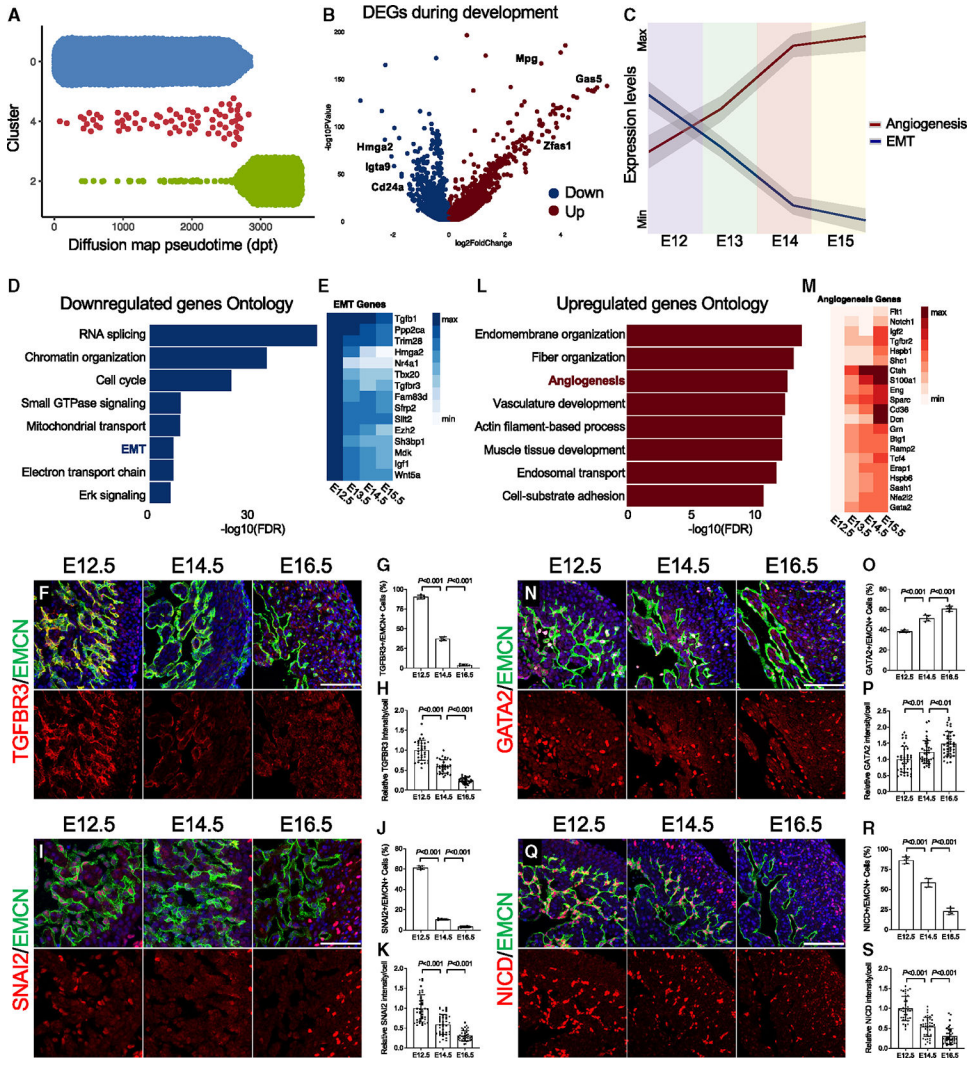

Figure 5. Developmentally regulated genes in ventricular endocardial cells involving EMT and angiogenesis

(A) Pseudotime trajectory analysis of endocardial cell clusters 0 and 4, and coronary endothelial cell cluster 2 shows cluster 4 as intermediate between main endocardial cells and coronary endothelial cells.

(B) Volcano plot shows developmentally downregulated (E12.5 > E13.5 > E14.5 > E15.5, blue) or upregulated (E12.5 < E13.5 < E14.5 < E15.5, red) genes in cluster 0 endocardial cells.

(C) Standardized average expression profiles of EMT and angiogenesis genes from E12.5 to E15.5 in cluster 0 endocardial cells.

(D) Enriched GO terms and pathways for developmentally downregulated genes from E12.5 to E15.5 in cluster 0 endocardial cells.

(E) Heatmap shows the relative expression in E13.5–E15.5 compared with E12.5 for genes in the EMT GO term.

(F–H) IF shows significantly decreased TGFBR3 expression (red) (F), TGFBR3-expressing cell percentage (G), and TGFBR3 expression intensity (H) in EMCN-expressing (green) ventricular endocardial cells from E12.5 to E16.5 (n = 5 hearts for each stage).
(I–K) IF shows significantly decreased SNAI2 expression (red) (I), SNAI2-expressing cell percentage (J), and SNAI2 expression intensity (K) in EMCN-expressing (green) ventricular endocardial cells from E12.5 to E16.5 (n = 5 hearts for each stage).
(L) Enriched GO terms and pathways for developmentally upregulated genes from E12.5 to E15.5 in cluster 0 endocardial cells.
(M) Heatmap shows the relative expression in E13.5–E15.5 compared with E12.5 for genes in the angiogenesis GO term.
(N–P) IF shows significantly upregulated GATA2 expression (red) (N), GATA2-expressing cell percentage (O), and GATA2 expression intensity (P) in EMCN-expressing (green) ventricular endocardial cells from E12.5 to E16.5 (n = 5 hearts for each stage).
(Q–S) IF shows significantly downregulated NICD expression (red) (Q), NICD-expressing cell percentage (R), and NICD expression intensity (S) in EMCN-expressing (green) ventricular endocardial cells from E12.5 to E16.5 (n = 5 hearts for each stage).
Scale bars: 100 μm. Error bars: SD. Statistical analysis was performed using two-tailed unpaired Student’s t tests. See also Figure S5.

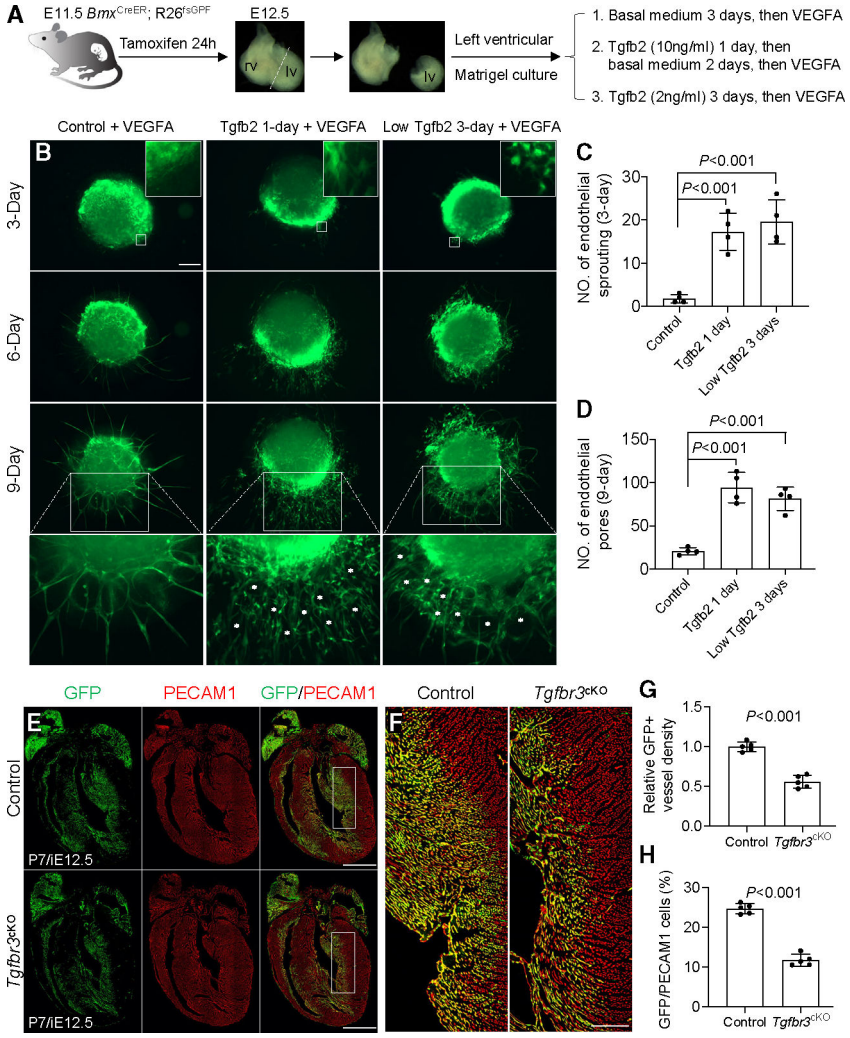

Figure 6. Ventricular endocardial cells form trabecular vessels by angioEMT

(A) Schematic shows Matrigel coronary angiogenesis assays using E12.5 left ventricular explants (rv, right ventricle; lv, left ventricle; dashed line indicates the sliced left ventricle for explant culture).

(B, top panel, and C) Show significantly induced angiogenic sprouting by GFP-expressing descendants from *Bmx*^{CreER} marked ventricular endocardial cells at E11.5 after TGFB2 treatment at day 3 culture.

(B, middle and bottom panels, and D) Show significantly promoted angiogenesis by GFP-expressing descendants from *Bmx*^{CreER} marked ventricular endocardial cells at E11.5 and formation of GFP-expressing vascular networks (asterisks) following subsequent VEGFA treatment at day 6–9 culture (n = 4 hearts for each group).

(E–H) IF shows significantly decreased trabecular-vessel density (G) and percentage of GPF-expressing (green)/PECAM1-expressing (red) coronary vessels at the left ventricle (H) of P7 *Tgfbr3*^{cKO} hearts.

Scale bars: 1,000 μm for (E); 100 μm for (B) and (F). Error bars: SD. Statistical analysis was performed using two-tailed unpaired Student's t tests. See also Figure S6.

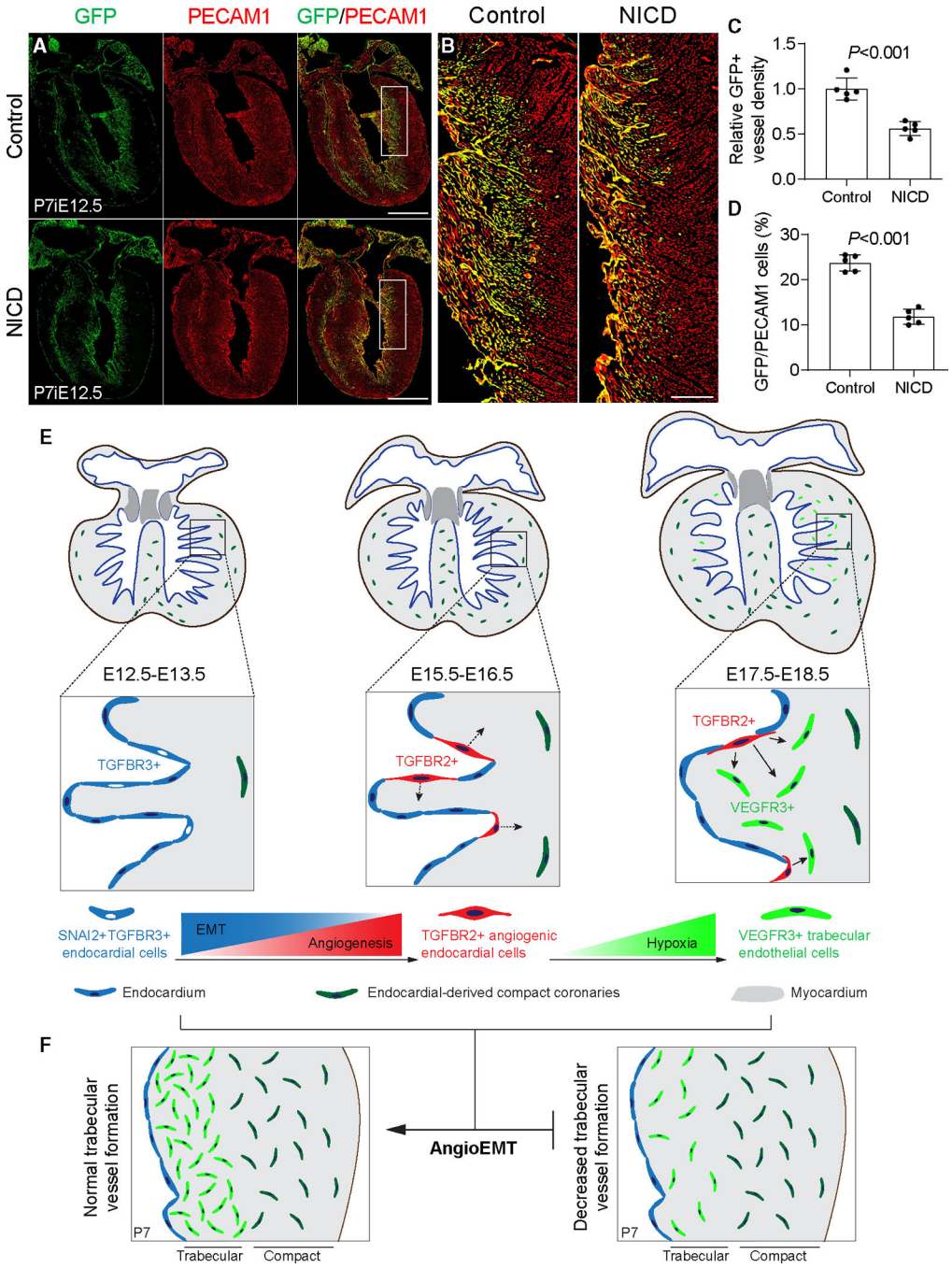

Figure 7. Two-step angioEMT model of trabecular-vessel formation by ventricular endocardial cells

(A–D) IF shows significantly decreased trabecular-vessel density (C) and percentage of GPF-expressing (green)/PECAM1-expressing (red) coronary vessels at the left ventricle (D) of P7 overexpressing NICD hearts. Simultaneous overexpression of NICD and GFP labeling of ventricular endocardial cells were achieved by induction of *Npr3*^{CreETR2} at E12.5 (iE12.5) (n = 5 hearts for each group).

(E and F) Diagram illustrating a two-step angioEMT model. (E) Ventricular endocardial cells form trabecular vessels by a unique EMT process, regulated by SNAI2-TGFB2/

TGFBR3 signaling, to become angiogenic fated progenitors. (F) These cells are subsequently activated by VEGFA-NOTCH1 signaling to undergo the second wave of coronary angiogenesis to form trabecular vessels.

Scale bars: 1,000 μm for (A); 200 μm for (B). Error bars: SD. Statistical analysis was performed using two-tailed unpaired Student's t tests. See also Figure S7.

KEY RESOURCES TABLE

REAGENT or RESOURCE	SOURCE	IDENTIFIER
Antibodies		
Anti-EMCN	Santa Cruz	Cat# sc-65495; RRID: AB_2100037
Anti-GFP	Abcam	Cat# ab6673; RRID: AB_305643
Anti-PECAM1	BD Pharmingen	Cat# 550274; RRID: AB_393571
Anti-NPR3	Santa Cruz	Cat# sc-515449; RRID: AB_2927802
Anti-IB4	Sigma	Cat# L-2140; RRID: AB_2313663
Anti-VEGFR3	R&D	Cat# AF743; RRID: AB_355563
Anti-SLUG	Cell Signaling	Cat# 9585S; RRID: AB_2239535
Anti-SNAIL	Cell Signaling	Cat# 3879S; RRID: AB_2255011
Anti-TWIST1	Santa Cruz	Cat# SC-81417; RRID: AB_1130910
Anti-TGFBR3	R&D	Cat# AF242-PB; RRID: AB_354417
Anti-GATA2	R&D	Cat# AF2046; RRID: AB_355123
Anti-N1ICD	Cell Signaling	Cat# 4147S; RRID: AB_2153348
Anti-HP1	Hypoxyprobe Inc	Cat# HP1–100Kit; RRID: AB_2811309
Anti-aSMA	Abcam	Cat# ab32575; RRID: AB_722538
Anti-PDGFRB	Abcam	Cat# ab32570; RRID: AB_777165
Anti-VIM	Abcam	Cat# ab92547; RRID: AB_10562134
Alexa Fluor-568 donkey anti-mouse IgG	Thermo Fisher Scientific	Cat# A10037; RRID: AB_2534013
Alexa Fluor-568 donkey anti-goat IgG	Thermo Fisher Scientific	Cat# A11057; RRID: AB_2534104
Alexa Fluor-488 donkey anti-goat IgG	Thermo Fisher Scientific	Cat# A11055; RRID: AB_2534102
Alexa Fluor-594 donkey anti-rat IgG	Thermo Fisher Scientific	Cat# A21209; RRID: AB_2535795
Alexa Fluor-488 donkey anti-rat IgG	Thermo Fisher Scientific	Cat# A21208; RRID: AB_2535794
Alexa Fluor-568 donkey anti-rabbit IgG	Thermo Fisher Scientific	Cat# A10042; RRID: AB_2534017
Alexa Fluor-488 donkey anti-rabbit IgG	Thermo Fisher Scientific	Cat# A21206; RRID: AB_2535792
Chemicals, peptides, and recombinant proteins		
Recombinant VEGFA120	R&D	Cat# 494-VE-025
Recombinant TGFB2	R&D	Cat# 7346-B2–005
Endothelial Cell Growth Basal Medium	R&D	Cat# CCM029
Tamoxifen	Sigma	Cat# T5648–1G
Matrigel® Growth Factor Reduced	Corning	Cat# 354230
Papain	Brainbits	Cat# pap
Critical commercial assays		
Chromium Single Cell 3' v2	10x Genomics	Cat# CG00052
Deposited data		
Deposited raw data files for Single-cell RNA-seq	This paper	GEO: GSE205394

REAGENT or RESOURCE	SOURCE	IDENTIFIER
Experimental models: Organisms/strains		
VegfA$^{f/f}$	Gerber et al.[24]	N/A
Tnt^{MerCreMer}	Yan et al.[23]	N/A
Npr3^{CreERT2}	Lu et al.[10]	N/A
Bmx^{CreER}	Ehling et al.[55]	N/A
R26^{fsGFP}	Miyoshi et al.[56]	N/A
Slug$^{-/-}$	Jiang et al.[43]	N/A
Tgfbr3$^{f/f}$	Li et al.[45]	N/A
R26^{fsN1ICD}	Murtaugh et al.[46]	N/A
Software and algorithms		
ImageJ	NIH	https://imagej.nih.gov/ij/
GraphPad Prism 8	GraphPad software	https://www.graphpad.com/scientific-software/prism/
Leica SP5 confocal microscope and imaging software	Leica	https://www.leica-microsystems.com/products/confocal-microscopes/p/leica-tcs-sp5/)
Cell Ranger (version 3.1.0)	10x Genomics	www.10xgenomics.com/
Seurat	Butler et al.[57]	www.satijalab.org/seurat/
ggplot2 (3.3.0)	N/A	https://ggplot2.tidyverse.org
CellChat	Jin et al.[26]	https://github.com/sqjin/CellChat
edgeR	N/A	https://bioconductor.org/packages/release/bioc/html/edgeR.html
clusterProfiler	N/A	https://bioconductor.org/packages/release/bioc/html/clusterProfiler.html
Destiny	Angerer et al.[58]	https://www.bioconductor.org/packages/release/bioc/html/destiny.html
Rrvgo	N/A	http://www.bioconductor.org/packages/release/bioc/html/rrvgo.html